J. Fluid Mech. (1981), *vol.* 112, *pp.* 1–32
Printed in Great Britain

Effects of nonlinearity and spectral bandwidth on the dispersion relation and component phase speeds of surface gravity waves

By DONALD R. CRAWFORD, BRUCE M. LAKE, PHILIP G. SAFFMAN† AND HENRY C. YUEN

Fluid Mechanics Department, TRW Defense and Space Systems Group, One Space Park, Redondo Beach, California 90278

(Received 22 September 1980 and in revised form 26 January 1981)

The dispersion relation and component phase speeds of surface gravity wavefields and modulated wavetrains are calculated. A parametric study is performed for a range of nonlinearity and spectral bandwidths. It is found that the amount of departure from linear theory increases with the ratio of nonlinearity to spectral bandwidth. The calculated results are compared quantitatively with laboratory and ocean measurements of wavetrains and wavefields with and without wind. The good agreement between theory and experiment suggests that the nonlinearity–dispersion balance is a likely candidate to account for the observed discrepancy between linear theory and data, as well as for the difference in behaviour between laboratory and oceanic wave measurements.

1. Introduction

Recent developments in the measurement and modelling of nonlinear wind waves have generated interest in the dispersion relation and component phase speeds of a spectrum of deep-water surface gravity waves. Open-ocean measurements by Von Zweck (1970), Yefimov, Solov'yev & Khristoforov (1972), Grose, Warsh & Garstang (1972) and Ramamonjiarisoa & Giovanangeli (1978), as well as laboratory measurements by Ramamonjiarisoa (1974), Ramamonjiarisoa & Coantic (1976), Lake & Yuen (1978), Rikiishi (1978) and Mitsuyasu, Kuo & Masuda (1979) all seem to indicate that some discrepancies exist between the measured values and the predictions of linear theory. The degree of departure from linear theory varies from case to case. Many explanations for this discrepancy have been proposed, including directional effects (Huang & Tung 1977), nonlinear effects of one form or another (Lake & Yuen 1978; Mollo-Christensen & Ramamonjiarisoa 1978; Yuen & Lake 1978; Grose *et al.* 1972; Masuda, Kuo & Mitsuyasu 1979) and surface drift current effects (Plant & Wright 1979). It is difficult to assess the relative merits of these explanations, for they all involve some assumptions about the wind-wave interaction process or the statistical properties of the wavefield – the rigour and validity of which are still open to question.

In this paper, an attempt is made to gain information on the properties of a gravity wavefield by calculating its dispersion relation and component phase speeds, in the simplest, yet non-trivial, situation. A one-dimensional, non-random, deep-water

† Applied Mathematics, California Institute of Technology, Pasadena, California.

gravity wavefield, in the absence of wind or currents, is examined. Even this apparently simple wave system displays a surprisingly rich structure, and provides important information on the dispersive properties of linear and nonlinear wavefields.

We recall two familiar results on deep-water waves. First, for a linear wave system, all components in the spectrum travel at different speeds, as given by the linear dispersion relation. Second, for a weakly nonlinear, uniform steady wavetrain (Stokes waves), all the harmonics travel at the same speed as the fundamental and hence they do not obey the linear dispersion relation. These results indicate that free linear waves and harmonics of a weakly nonlinear wavetrain can behave quite differently. In general, for a system of waves which are not infinitesimal, both free waves and harmonics (bound waves) exist, and an important issue to be resolved is how the nonlinearity and bandwidth of a wave system affect the dispersive behaviour of a particular wave component. The integral equation first derived by Zakharov (1968) is used as the governing equation for the evolution of the wave field. Zakharov showed that this equation reduces to the nonlinear Schrödinger equation, if one assumes a narrow bandwidth and a constant dominant wavenumber. Crawford, Saffman & Yuen (1980) extended Zakharov's equation to describe the evolution of a random wavefield possessing spatial inhomogeneity, and showed that the results were consistent with those of Hasselmann (1962, 1963) when the wave field was assumed homogeneous. Crawford *et al.* (1981) examined the stability properties of a nonlinear wavetrain using Zakharov's equation, and found that significant differences from results obtained by Benjamin & Feir (1967) exist for moderate and large values of wave steepness ($k_0 a_0$, where k_0 is the carrier wavenumber and a_0 is the carrier wave amplitude). Saffman & Yuen (1978), using a multiple time-scale approach, demonstrated that, when the ratio of the bandwidth of the spectrum to the characteristic nonlinearity of the wave system is of order unity or less, the lower-order mechanisms contained in Zakharov's equation dominate. When the ratio is very large, effects of these lower-order mechanisms diminish, and the wave system behaves in a near-linear fashion to the order considered. Thus, Zakharov's equation adequately describes the evolution of a nonlinear wavetrain (and provides a better model than the nonlinear Schrödinger equation), and it is consistent with the known results for linear or near-linear spectra of waves. This makes it an appropriate equation on which to base this study.

Section 2 will briefly describe the governing equation for the evolution of a wavefield. Section 3 defines the procedure for determining the component phase speeds and dispersion relation of a wavefield. Results of the calculation are given in §§4 and 5 and these results are compared with available experimental data in §6. A discussion and summary are provided in §7.

2. The governing equations

It has been shown by Zakharov (1968) that the equation governing the evolution of a field of weakly nonlinear, deep-water, gravity waves is

$$i\frac{\partial A(\mathbf{k},t)}{\partial t} = \iiint_{-\infty}^{\infty} T(\mathbf{k},\mathbf{k}_1,\mathbf{k}_2,\mathbf{k}_3)\,\delta(\mathbf{k}+\mathbf{k}_1-\mathbf{k}_2-\mathbf{k}_3)\,e^{i[\omega(\mathbf{k})+\omega(\mathbf{k}_1)-\omega(\mathbf{k}_2)-\omega(\mathbf{k}_3)]t} \times A^*(\mathbf{k}_1,t)\,A(\mathbf{k}_2,t)\,A(\mathbf{k}_3,t)\,d\mathbf{k}_1\,d\mathbf{k}_2\,d\mathbf{k}_3, \quad (1)$$

where ( )* denotes complex conjugation; $\mathbf{k} = (k, l)$ is the wave vector; $\mathbf{x} = (x, y)$ is the spatial vector; $\omega(\mathbf{k})$ is the linear wave frequency, defined as

$$\omega(\mathbf{k}) = (g|\mathbf{k}|)^{\frac{1}{2}}, \tag{2}$$

with g as the acceleration due to gravity; $T(\mathbf{k}, \mathbf{k}_1, \mathbf{k}_2, \mathbf{k}_3)$ is a real, scalar interaction coefficient first calculated by Zakharov (1968), and is recorded in appendix A with some minor algebraic errors removed.

The free surface $\eta(\mathbf{x}, t)$ is specified by $A(\mathbf{k}, t)$ through the following expressions:

$$\eta(\mathbf{x}, t) = \frac{1}{2\pi\sqrt{2}} \int_{-\infty}^{\infty} \left(\frac{|\mathbf{k}|}{\omega(\mathbf{k})}\right)^{\frac{1}{2}} [a(\mathbf{k}, t)\, e^{i\mathbf{k}\cdot\mathbf{x}} + a^*(\mathbf{k}, t)\, e^{-i\mathbf{k}\cdot\mathbf{x}}]\, d\mathbf{k}, \tag{3}$$

$$a(\mathbf{k}, t) = [A(\mathbf{k}, t) + B(\mathbf{k}, t)]\, e^{-i\omega(\mathbf{k})t}, \tag{4}$$

$$\begin{aligned} B(\mathbf{k}, t) = -\iint_{-\infty}^{\infty} \Bigg\{ & V^{(-)}(\mathbf{k}, \mathbf{k}_1, \mathbf{k}_2)\, A(\mathbf{k}_1, t)\, A(\mathbf{k}_2, t)\, \delta(\mathbf{k} - \mathbf{k}_1 - \mathbf{k}_2) \left[\frac{e^{i[\omega(\mathbf{k}) - \omega(\mathbf{k}_1) - \omega(\mathbf{k}_2)]t} - 1}{\omega(\mathbf{k}) - \omega(\mathbf{k}_1) - \omega(\mathbf{k}_2)}\right] \\ & + 2\, V^{(-)}(\mathbf{k}, \mathbf{k}_1, \mathbf{k}_2)\, A(\mathbf{k}_1, t)\, A^*(\mathbf{k}_2, t)\, \delta(\mathbf{k} - \mathbf{k}_1 + \mathbf{k}_2) \left[\frac{e^{i[\omega(\mathbf{k}) - \omega(\mathbf{k}_1) + \omega(\mathbf{k}_2)]t} - 1}{\omega(\mathbf{k}) - \omega(\mathbf{k}_1) + \omega(\mathbf{k}_2)}\right] \\ & + V^{(+)}(\mathbf{k}, \mathbf{k}_1, \mathbf{k}_2)\, A^*(\mathbf{k}_1, t)\, A^*(\mathbf{k}_2, t)\, \delta(\mathbf{k} + \mathbf{k}_1 + \mathbf{k}_2) \left[\frac{e^{i[\omega(\mathbf{k}) + \omega(\mathbf{k}_1) + \omega(\mathbf{k}_2)]t} - 1}{\omega(\mathbf{k}) + \omega(\mathbf{k}_1) + \omega(\mathbf{k}_2)}\right] \Bigg\} \\ & \times d\mathbf{k}_1\, d\mathbf{k}_2, \end{aligned} \tag{5}$$

where $B(\mathbf{k}, t)$ is the second-order correction to $A(\mathbf{k}, t)$ and $V^{(\pm)}(\mathbf{k}, \mathbf{k}_1, \mathbf{k}_2)$ are real, scalar, second-order interaction coefficients given in appendix A. The free-surface representation given by equations (3), (4) and (5) is correct to second order in wave amplitude.

3. Calculation of component phase speeds and dispersion relation for a spectrum of waves

This study will henceforth focus on one-space dimensional situations, but the generalization of two-space dimensions presents no conceptual difficulties. For a given free surface $\eta(x, t)$, a bandpass filtering process is defined as one which yields a filtered signal $\tilde{\eta}_p(x, t)$ for each selection of wavenumber k_p:

$$\tilde{\eta}_p(x, t) = \int_{-\infty}^{\infty} \eta(x + \xi, t)\, K_p(\xi)\, d\xi, \tag{6}$$

where

$$K_p(\xi) = \frac{4 \cos(k_p \xi) \sin(\Delta_f \xi)}{\xi}. \tag{7}$$

The filter function $K_p(\xi)$ as defined in (7) corresponds to a top-hat filter with total bandwidth $2\Delta_f$ centred at k_p, which is evident from the properties of its Fourier transform $\hat{K}_p(\kappa)$:

$$\hat{K}_p(\kappa) = \frac{1}{2\pi} \int_{-\infty}^{\infty} e^{i\kappa\xi}\, K_p(\xi)\, d\xi = \begin{cases} 1, & |\kappa - k_p| < \Delta_f; \\ 0, & \text{elsewhere.} \end{cases} \tag{8}$$

A space–time correlation function $R_p(\lambda, \tau)$ is defined for the filtered signals:

$$R_p(\lambda, \tau) = \langle \tilde{\eta}_p(x, t)\, \tilde{\eta}_p(x + \lambda, t + \tau) \rangle, \tag{9}$$

where $\langle\ \rangle$ denotes ensemble averaging, and the processes are assumed to be statistically homogeneous and stationary so that R_p is independent of x and t. For a fixed value of τ, say τ_0, let λ_m satisfy

$$\frac{d}{d\lambda} R_p(\lambda_m, \tau_0) = 0, \tag{10}$$

which is the lag-distance to maximum correlation for a well-defined correlation function. The phase velocity $C(k_p)$ is then defined by

$$C(k_p) = \lim_{\tau_0 \to 0} \frac{\lambda_m}{\tau_0}; \tag{11}$$

the corresponding frequency $\Omega(k_p)$ is

$$\Omega(k_p) = C(k_p)\, k_p. \tag{11a}$$

The above procedure is now applied to a wavefield characterized by a given $A(k,t)$. In general, experimental measurements of η and $d\eta/dt$ at a given time determine a and a^*; from which the complex-valued function A would follow, after solving an integral equation given by (4) and (5). Of concern presently, however, are the effects of nonlinearity and spectral bandwidth on the component phase speeds and dispersion relation; for this purpose, exact details of A are unimportant and it is sufficient to consider real, prescribed functional forms for A. Note that, even when A is real, the second-order correction B [defined in terms of A in equation (5)] is generally complex.

Substitution of equations (3) and (4) into (6), and taking the limit of small Δ_f, yields $\tilde{\eta}_p(x,t)$ in terms of A and B:

$$\begin{aligned}\tilde{\eta}_p(x,t) = {} & \frac{2}{\sqrt{2}} \frac{k_p^{\frac{1}{2}}}{\omega_p^{\frac{1}{2}}} \Delta_f A(k_p,t) \cos(k_p x - \omega_p t) + \frac{1}{\sqrt{2}} \frac{k_p^{\frac{1}{2}}}{\omega_p^{\frac{1}{2}}} \Delta_f [B(-k_p,t) \exp[-i(k_p x + \omega_p t)] \\ & + B^*(-k_p,t) \exp[i(k_p x + \omega_p t)] + B(k_p,t) \exp[i(k_p x - \omega_p t)] \\ & + B^*(k_p,t) \exp[-i(k_p x - \omega_p t)]],\end{aligned} \tag{12}$$

where $\omega_p = \omega(k_p) = (gk_p)^{\frac{1}{2}}$. The stationarity assumption permits us to choose $x = t = 0$, and condition (10) reduces to

$$\frac{d}{d\lambda} \tilde{\eta}_p(\lambda, \tau_0)\Big|_{\lambda = \lambda_m} = 0. \tag{13}$$

Direct evaluation of (13) using expression (12) gives

$$C(k_p) = \frac{\omega_p [A(k_p) + B_r(k_p) - B_r(-k_p)]}{k_p [A(k_p) + B_r(k_p) + B_r(-k_p)]} \frac{-\operatorname{Im}\left[\dfrac{\partial A}{\partial t}(k_p)\right] - \dfrac{\partial B_i}{\partial t}(k_p) - \dfrac{\partial B_i}{\partial t}(-k_p)}{k_p [A(k_p) + B_r(k_p) + B_r(-k_p)]}, \tag{14}$$

where Im[ ] denotes the imaginary part, B_r and B_i are the real and imaginary parts of B, $\partial A(k_p, 0)/\partial t$ is given by equation (1), and $\partial B_i(\pm k_p, 0)/\partial t$ is given in appendix B.

For a linear wavefield, the higher-order correction terms B, $\partial A/\partial t$ and $\partial B_i/\partial t$ are all negligible, and $C(k_p)$ reduces to the linear result

$$C(k_p) = \frac{\omega_p}{k_p}, \tag{15}$$

regardless of the structure of the spectrum. Stokes' result for a weakly nonlinear wavetrain can be recovered by taking

$$A(k) = b_0 \delta(k - k_0). \tag{16}$$

Letting $k_p = k_0$, the equation obtained is

$$\tilde{\eta}_p(\lambda, \tau) = \frac{1}{\sqrt{2}} \frac{k_0^{\frac{1}{2}}}{\omega_0^{\frac{1}{2}}} [2b_0 \cos(k_0\lambda - \omega_0\tau) + 2\tau T(k_0, k_0, k_0, k_0) b_0^3 \sin(k_0\lambda - \omega_0\tau)], \tag{17}$$

where

$$T(k_0, k_0, k_0, k_0) = \frac{k_0^3}{4\pi^2}, \tag{18}$$

and b_0 is related to the amplitude of the wavetrain a_0 by

$$b_0^2 = \frac{2\pi^2 a_0^2 \omega_0}{k_0}. \tag{19}$$

For a given τ_0, the condition

$$\left.\frac{d\tilde{\eta}_p}{d\lambda}\right|_{\lambda=\lambda_m} = 0, \tag{20}$$

yields the phase speed $C(k_0)$ as

$$\begin{aligned} C(k_0) &= \frac{\omega_0}{k_0} + \frac{T(k_0, k_0, k_0, k_0) b_0^2}{k_0} \\ &= \frac{\omega_0}{k_0}(1 + \tfrac{1}{2}k_0^2 a_0^2), \end{aligned} \tag{21}$$

which is the phase speed of the fundamental mode of a weakly nonlinear wavetrain obtained by Stokes.

When $k_p = 2k_0$ is taken, a similar calculation gives

$$C(2k_0) = \frac{\omega_0}{k_0}(1 + \tfrac{1}{2}k_0^2 a_0^2), \tag{22}$$

indicating that the second harmonic travels at the phase speed of the fundamental mode. This result serves to check our formulations, since all harmonics of a steady wavetrain must travel at the same speed.

4. Results for a modulated wavetrain

In this section, some results of the dispersion-relation and component-phase-speed calculations for a modulated wavetrain are presented. The form of $A(k)$ is chosen to be

$$A(k) = b_0 \delta(k - k_0) + b_+ \delta(k - k_0 - \Delta k_0) + b_- \delta(k - k_0 + \Delta k_0), \tag{23}$$

which corresponds to a dominant component of strength b_0 at $k = k_0$ and a pair of sidebands with strengths $b_\pm$ (small compared with b_0), located at $\pm\Delta k_0$ away from the dominant component. The degree of modulation is proportional to the sideband strengths, and the wavelength of modulation is inversely proportional to the sideband separation. These three components form the primary system. Second-order corrections are given by equation (5), and yield secondary 'forced' components at $k = \Delta k_0$, $2\Delta k_0$, $2k_0 - 2\Delta k_0$, $2k_0 - \Delta k_0$, $2k_0$, $2k_0 + \Delta k_0$, $2k_0 + 2\Delta k_0$. The component at Δk_0 describes the wave envelope and should travel with the group velocity, which to leading order is one-half of the value for the phase velocity. The component at $2\Delta k_0$ does not possess

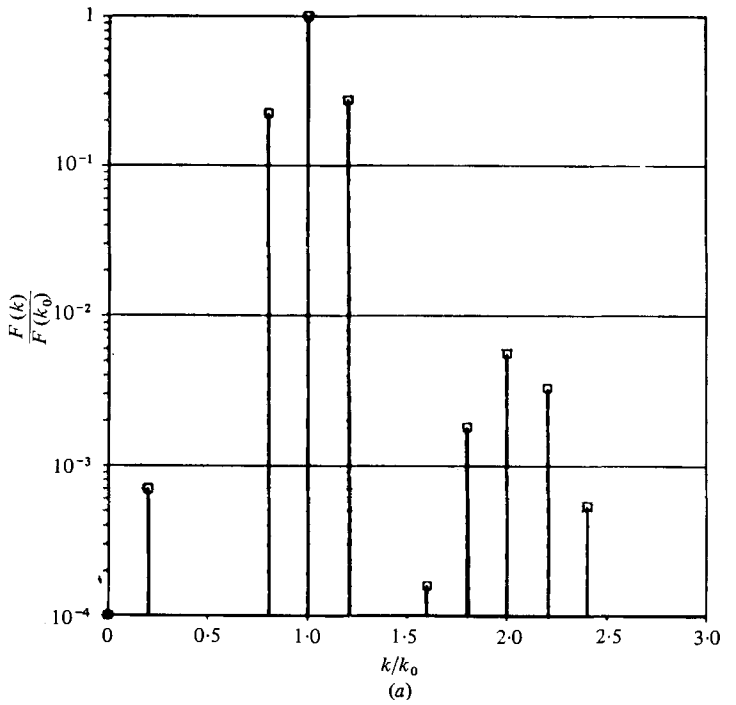

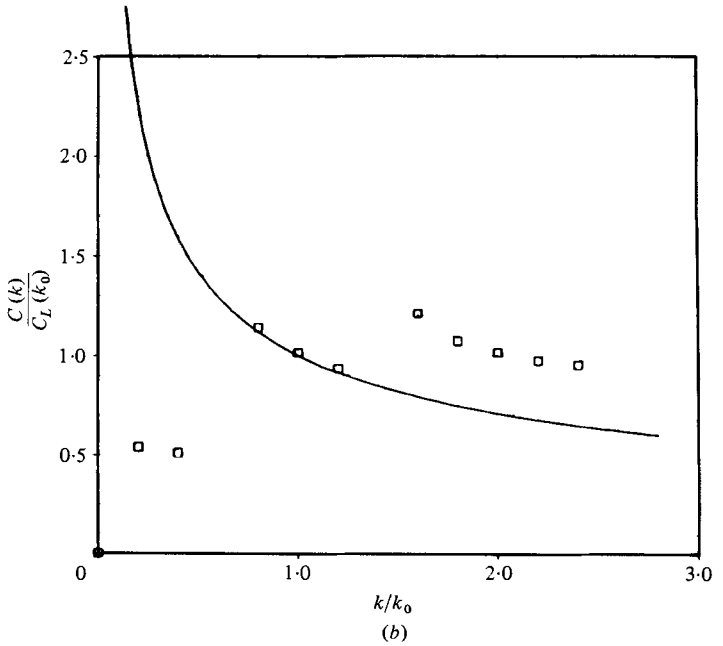

FIGURE 1. Phas-espeed calculations for a modulated wavetrain with $(ka)_{\text{rms}} = 0{\cdot}10$. (*a*) Dimensionless spectrum $F(k)/F(k_0)$ versus dimensionless wavenumber k/k_0. (*b*) Component phase speed normalized by linear phase speed k_0, $C(k)/C_L(k_0)$, versus dimensionless wavenumber k/k_0. ——, linear case.

a familiar physical interpretation, but should behave in a similar manner as the component at Δk_0. The component at $k = 2k_0$ is the second harmonic, and the four neighbouring components reflect the effect of the modulation on the second harmonic.

A plot of the resulting spectrum $F(k) = A(k) + B(k)$, corresponding to a case where the root-mean-square wave steepness $(ka)_{\text{rms}} = 0{\cdot}10$, $\Delta = 0{\cdot}2$ and $b_{\pm}/b_0 = 0{\cdot}1$, is given in figure 1 (*a*). All components mentioned above can be seen except the one at $2\Delta k_0$, which is too small to appear on the same scale. The inequality of the sideband components is caused by the k-dependent normalization in the definition of $A(k)$. The inequality of the neighbouring components of the second harmonic results from this normalization effect, as well as the k-dependence of the interaction coefficient appearing in equation (5).

In figure 1 (*b*) the component phase speeds $C(K)$ are plotted [normalized by the linear phase speed based on the dominant wavenumber, $C_L(k_0)$] against the wavenumber (normalized by the peak wavenumber k_0). It can be seen that the component phase speeds of the primary system of wave components (at $k/k_0 = 1{\cdot}0$, $0{\cdot}8$ and $1{\cdot}2$) follow closely those obtained from the linear dispersion relation (represented by the solid line), with minor corrections $(ka)^2_{\text{rms}}$ due to the nonlinearity. The low-wavenumber components at Δk_0 and $2\Delta k_0$ stay near the group velocity value at approximately one-half of the primary phase speed. The second harmonic at $2k_0$ travels at the same speed as the primary, and its neighbouring components behave in a manner similar to that of the sidebands of the dominant wave. Thus, the 'forced' components do not follow the linear dispersion relation results, but instead behave in a manner expected of a nonlinearly coupled wave system.

A second example of results obtained for modulated wavetrains is given in figure 2. All parameters remain the same as in figure 1 except that $(ka)_{\text{rms}}$ is now $0{\cdot}01$, so the wavetrain can be considered linear for almost all practical purposes. The power spectrum is shown in figure 2 (*a*); all the 'forced' components including the second harmonic are too small to appear in the plot. The plot of the normalized component phase speeds against the normalized wavenumber, however, shows substantially the same trend as that found in figure 1 (*b*) (see figure 2*b*). The low-wavenumber components travel at group speed, and the second harmonic at the same speed as the dominant. The sidebands of the dominant component follow the linear theory closely, and the neighbouring components of the second harmonic have the same trend as those in the primary system. Despite the extremely weak nonlinearity, none of the forced components obey the linear theory.

Other related results are shown in figures 2 (*c*)–(*g*). The dispersion relation showing the frequency (normalized by the linear frequency at k_0) against the normalized wavenumber is given in figure 2 (*c*). The normalized phase speed is plotted against the normalized frequency in figure 2 (*d*). In figures 2 (*e*)–(*g*), the above plots are repeated, but with normalization based on the peak values and not the linear results at the peak wavenumber. In the subsequent presentation of results, the latter normalization will be used.

These results apply only to the primary components and their second harmonics, do not take into consideration the behaviour of third and higher harmonics. However, most of the present conclusions can be extrapolated to higher harmonics without substantial qualitative changes. For example, a higher-order analysis would lead to the result that all the harmonics generated by the primary system travel at

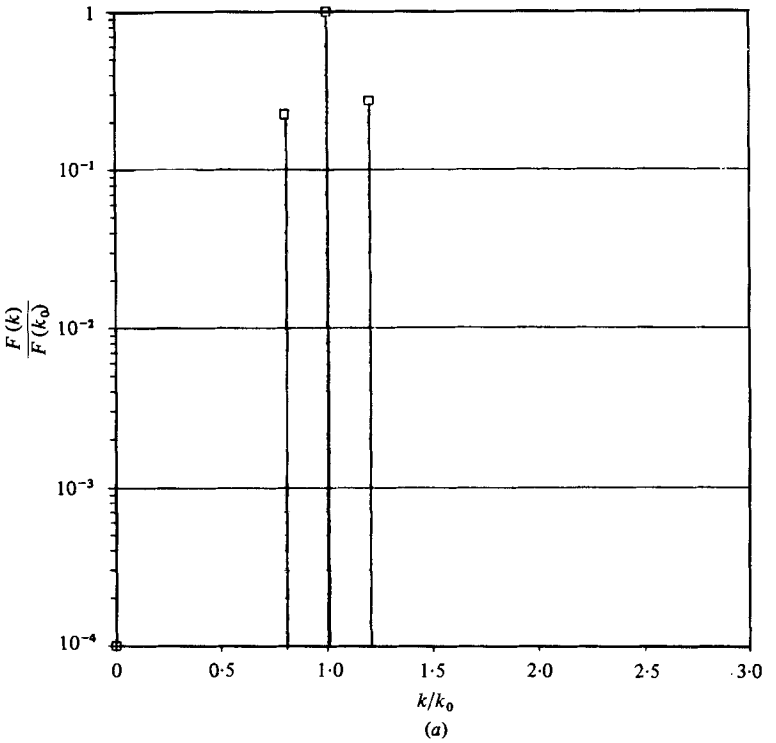

(*a*)

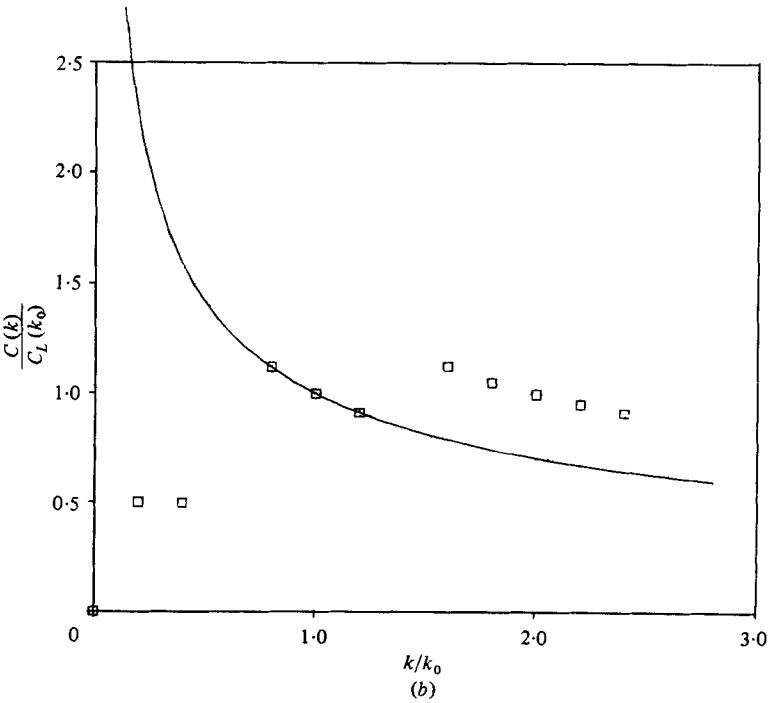

(*b*)

For legend for 2(*a*), (*b*) see p. 11.

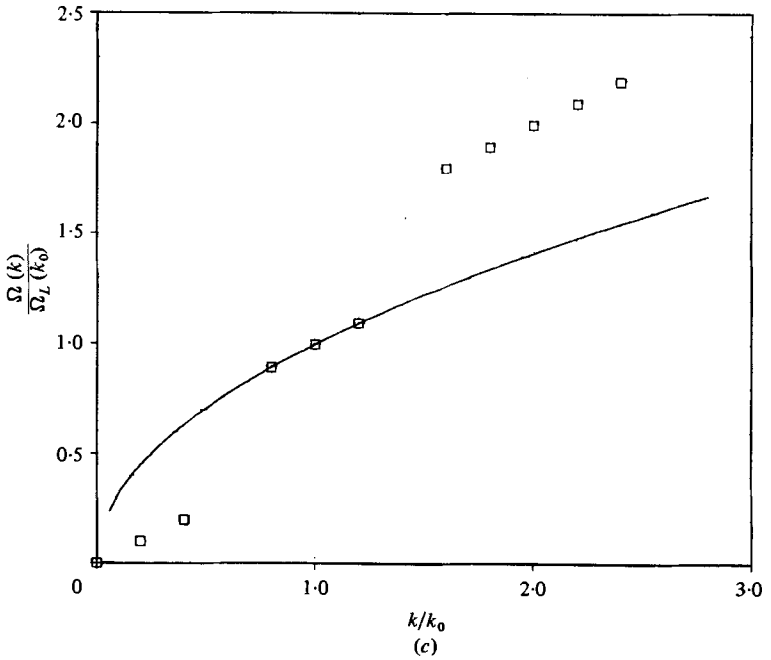

(*c*)

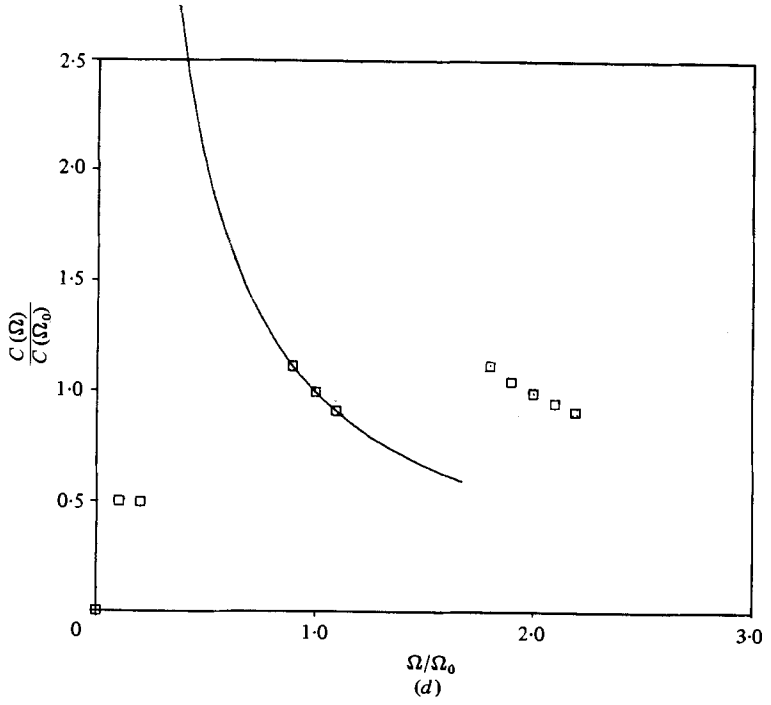

(*d*)

For legend for 2(*c*), (*d*) see p. 11.

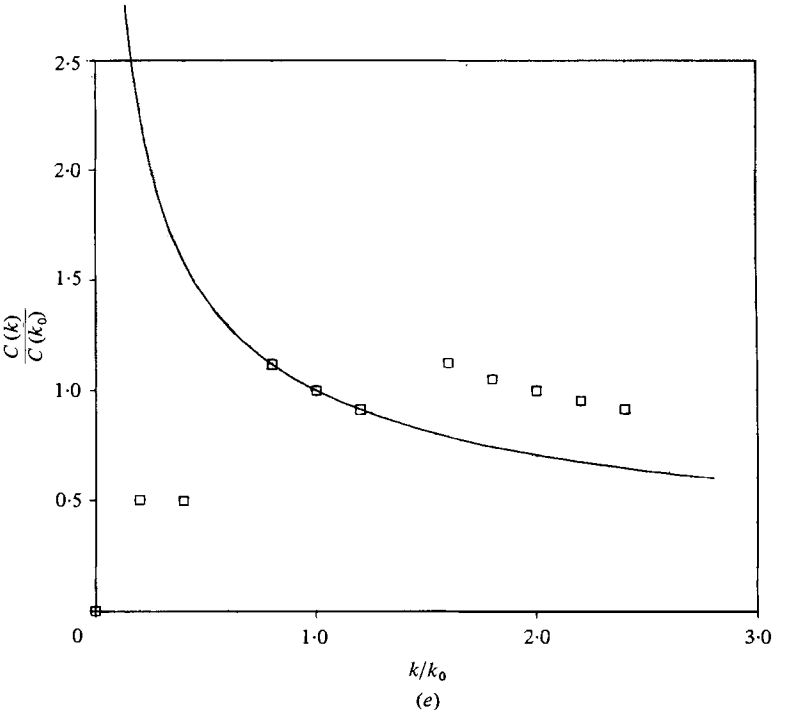

(*e*)

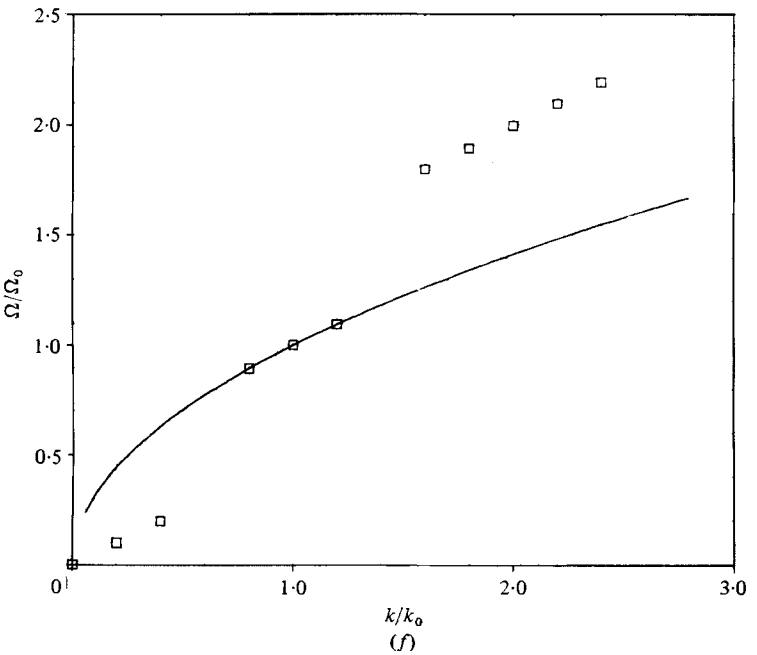

(*f*)

For legend for 2(*e*), (*f*) see p. 11.

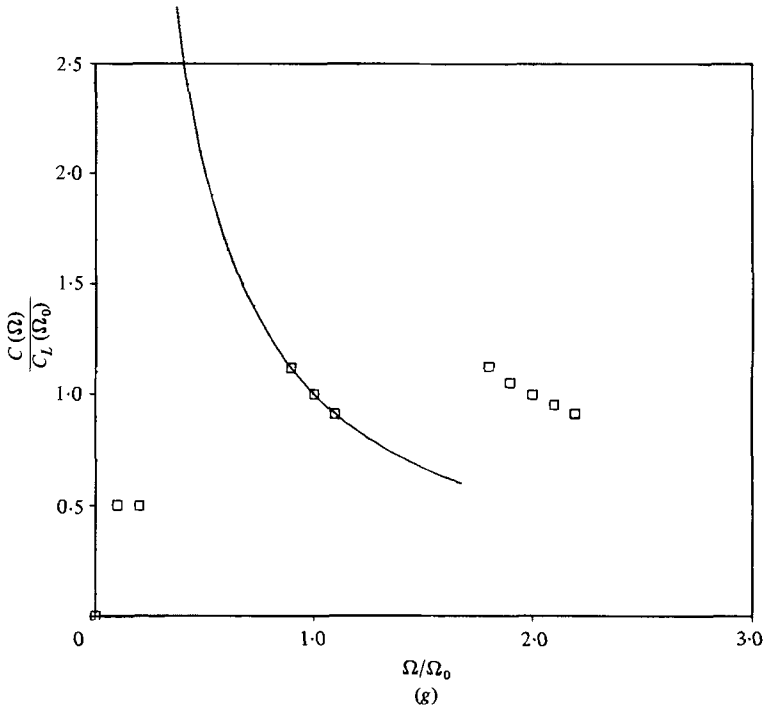

FIGURE 2. Phase-speed and dispersion-relation calculations for a modulated wavetrain with $(ka)_{rms} = 0{\cdot}01$. (*a*) Dimensionless spectrum $F(k)/F(k_0)$ versus dimensionless wavenumber k/k_0. (*b*) Component phase speed normalized by linear phase speed at k_0, $C(k)/C_L(k_0)$, versus dimensionless wavenumber k/k_0. (*c*) Dispersion relation: dimensionless frequency normalized by linear theory $\Omega(k)/\Omega_L(k_0)$, versus wavenumber k/k_0. (*d*) Dimensionless component phase speed normalized by linear theory $C(\Omega)/C_L(\Omega_0)$ versus normalized frequency Ω/Ω_0. (*e*) Component phase speed normalized by phase speed at k_0, $C(k)/C(k_0)$, versus dimensionless wavenumber k/k_0. (*f*) Dispersion relation: Dimensionless frequency normalized by frequency at k_0, $\Omega(k)/\Omega(k_0)$, versus dimensionless wavenumber k/k_0. (*g*) Dimensionless component phase speed normalized by value at k_0, $C(\Omega)/C(\Omega_0)$, versus dimensionless wavenumber Ω/Ω_0. ——, linear case.

the same speed as the dominant wave. The behaviour of the components near the generated higher harmonics is expected to follow that of the components in the vicinity of the second harmonic at least qualitatively. Taking this expectation further, more forced components should be found around higher harmonics, and their dependence on wavenumber should be weaker and weaker; this is evidenced by the fact that the dependence on wavenumber of the components around the second harmonic is weaker than that around the dominant wave (see figures 2(*b*), (*g*) for frequency dependence). As a result, the plot of the component phase speed, against wavenumber or frequency, should level out at the dominant wave speed at higher wavenumbers or frequencies. The same tendency is noted by Ramamonjiarisoa & Coantic (1976) and Lake & Yuen (1978) for a wind-generated wave field in a one-dimensional wave tank, which suggests the existence of forced components (or 'bound' waves). It must be kept in mind, however, that in a situation where the waves are generated by a complicated disturbance (such as wind) the higher modes are composed of free waves as well as forced components, and the resulting dispersion-relation and phase-speed

plots will reflect mixed behaviour. In the next section, some examples are presented to illustrate the nature of these mixed systems by considering spectra of waves.

5. Results for spectra with varying nonlinearity and bandwidth

We now consider continuous spectra. The leading-order spectrum $A(k)$ is assumed to take the form of a Lorentzian distribution, with a decay rate of k^{-4}. The spectral form is completely specified by two parameters governing the effective bandwidth and the characteristic nonlinearity, the definition of which are given in appendix C.

We first examine the effects of nonlinearity by varying $(ka)_{\rm rms}$ while keeping the bandwidth σ constant. Figure 3 shows a series of calculations for a relatively narrow spectrum ($\sigma = 0{\cdot}05$) for three values of $(ka)_{\rm rms}$: 0·01, 0·10 and 0·20. The plots for $F(k) = A(k) + B(k)$ are given in figure 3(*a*). It can be seen that the second harmonic becomes more prominent as $(ka)_{\rm rms}$ increases. The component phase speed (normalized by its value at the spectral peak) is plotted against the wavenumber (normalized by the wavenumber at the spectral peak) for each of the three cases in figure 3(*b*). For small nonlinearity [$(ka)_{\rm rms} = 0{\cdot}01$], the departure from the linear results is concentrated at the second harmonic region. The departure becomes more significant, and at the same time less localized, as nonlinearity increases. The plot of component phase speed against frequency (normalized by the frequency associated with the peak wavenumber) is shown in figure 3(*c*). Again, the departure from linear theory increases in magnitude and spread as nonlinearity increases. The interesting point to note here is that the location of the departure from linear theory moves from a value close to $\Omega/\Omega_0 = 1{\cdot}6$ for $(ka)_{\rm rms} = 0{\cdot}01$ to $\Omega/\Omega_0 = 2{\cdot}0$ for $(ka)_{\rm rms} = 0{\cdot}2$. The reason for this behaviour can be found in the dispersion relation given in figure 3(*d*), which shows the departure from linear dispersion relation with increasing nonlinearity. For $(ka)_{\rm rms} = 0{\cdot}01$, the departure for linear theory is small, so that $\Omega/\Omega_0 = (k/k_0)^{\frac{1}{2}}$; thus $k/k_0 = 2$ corresponds roughly to $\Omega/\Omega_0 = \sqrt{2}$. For stronger nonlinearity, the dispersion curve approaches that for a dispersionless system, and $k/k_0 = 2$ then corresponds to $\Omega/\Omega_0 = 2$. The same reasoning also applies to explain the apparent difference in the lengths of the phase speed curves (figure 3*c*) for various values of nonlinearity.

The results for a relatively broad spectrum ($\sigma = 0{\cdot}2$) are given in figure 4. The departure is more spread out compared to the narrow band case. The dispersion relation in figure 4(*d*) again shows the tendency towards a dispersionless behaviour as nonlinearity increases.

The next series of calculations concerns the effects of bandwidth for fixed nonlinearity. Figure 5 shows the results for $(ka)_{\rm rms} = 0{\cdot}01$ and σ varies from 0·05 to 0·30. The plots of $F(k) = A(k) + B(k)$ indicate that the second harmonic is obscured in all but the most narrow band case. The component phase speed approximates closely that given by the linear theory, with a small localized departure for the narrow-band case. The departures are negligible for the other cases. Similar conclusions can be drawn from the phase speed/frequency plot and the dispersion relation. The strong nonlinearity case, with $(ka)_{\rm rms} = 0{\cdot}2$, is shown in figure 6. The prominence of the second harmonic again decreases with increasing bandwidth (figure 6*a*). However, the component phase speed (figures 6*b*, *c*) and the dispersion relation (figure 6*d*) are quite insensitive to the variation in bandwidth despite the rather striking differences in spectral appearance.

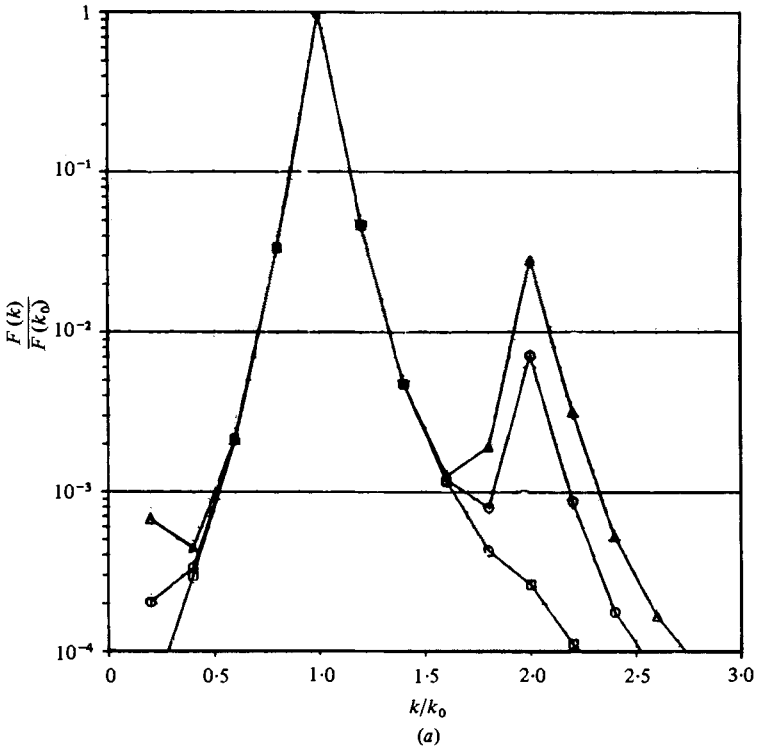

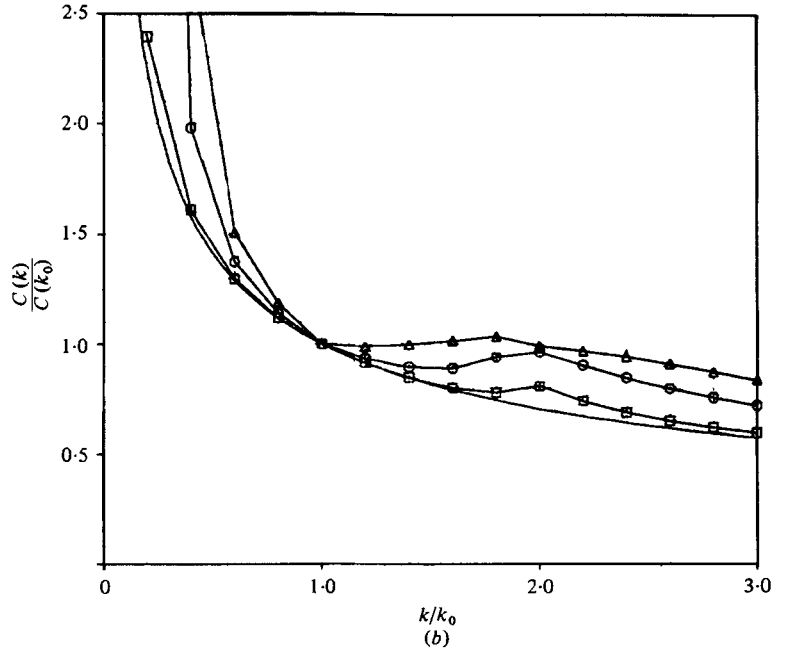

For legend for 3(*a*), (*b*) see p. 14.

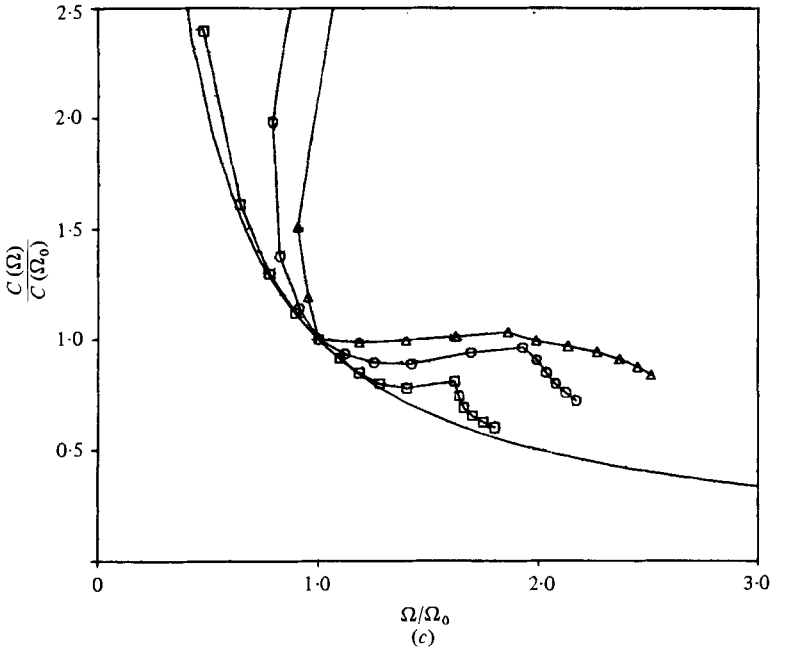

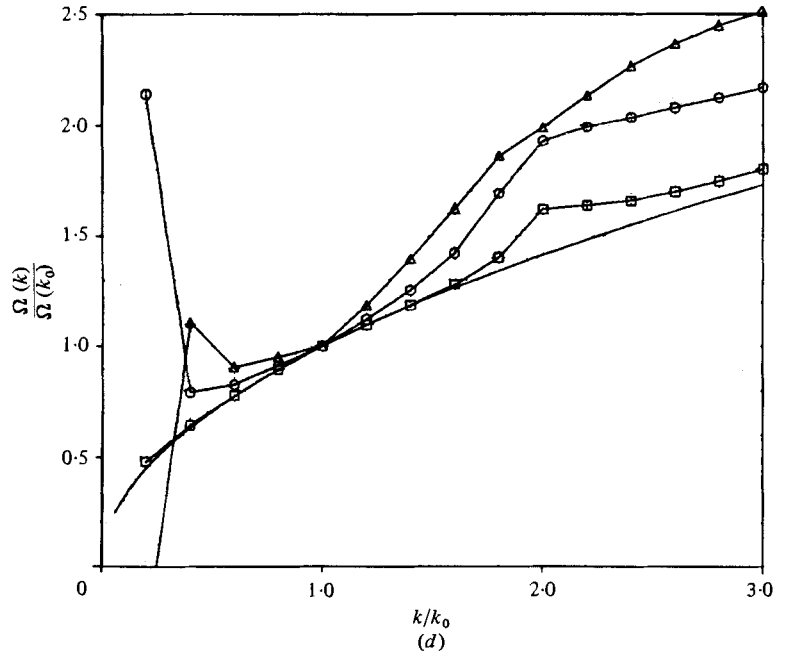

FIGURE 3. Component-phase-speed and dispersion-relation calculations for continuous spectra (Lorentzian form) with fixed bandwidth, $\sigma = 0{\cdot}05$ and varying nonlinearity. (*a*) Dimensionless wavenumber spectra. (*b*) Normalized component phase speed as a function of wavenumber. (*c*) Normalized component phase speed as a function of frequency. (*d*) Normalized dispersion relation. □, $ka = 0{\cdot}01$; ○, $ka = 0{\cdot}10$; △, $ka = 0{\cdot}20$. ——, linear case.

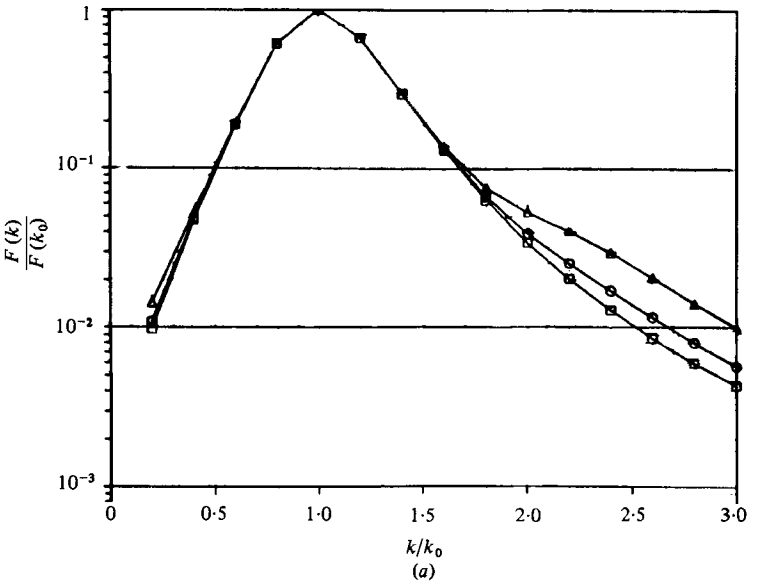

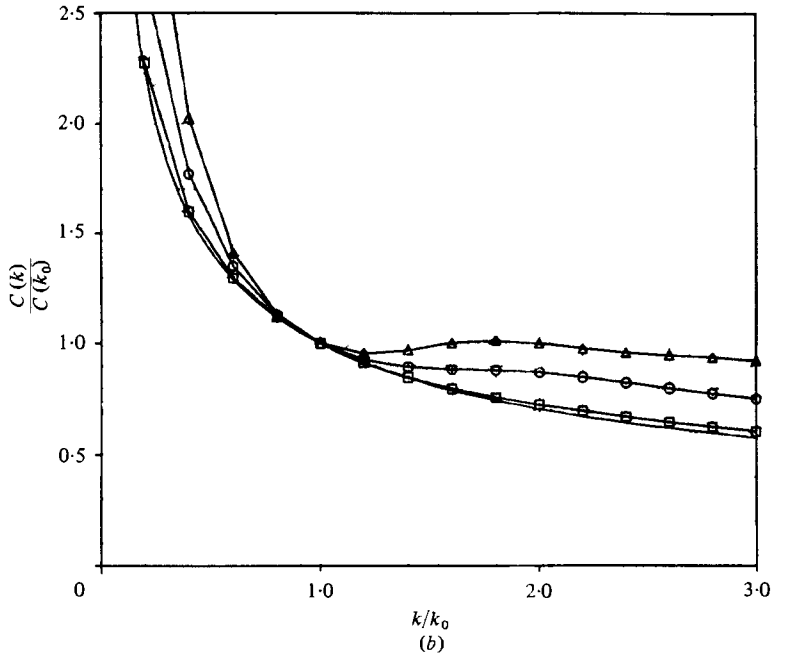

For legend for 4(*a*), (*b*) see p. 16.

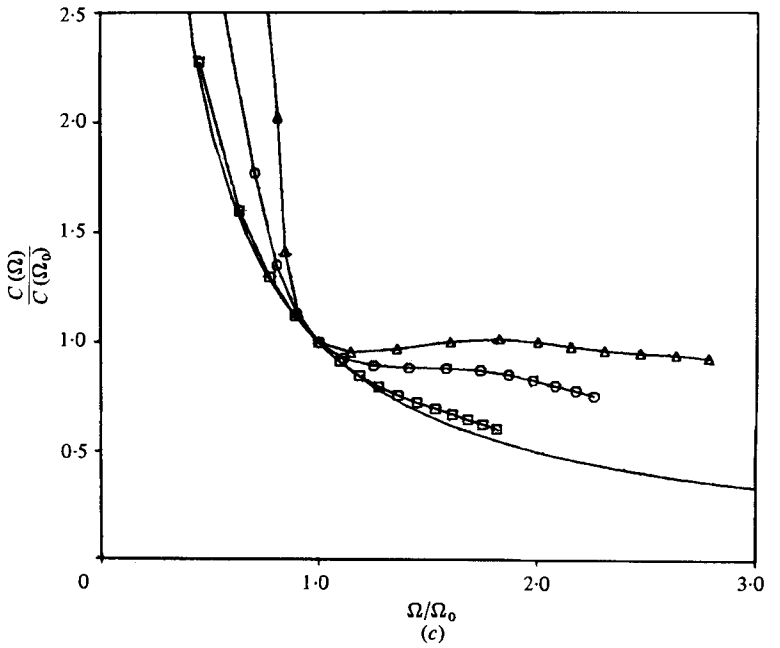

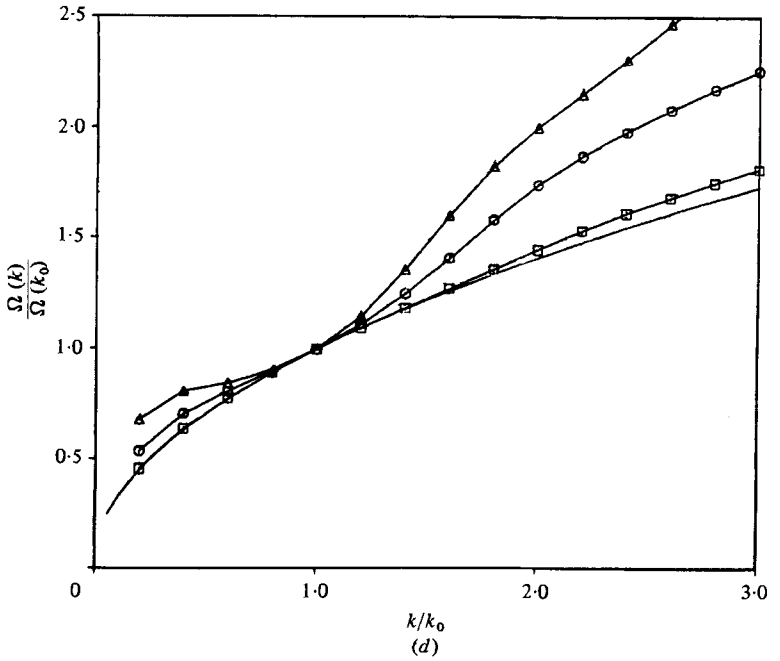

FIGURE 4. Component-phase-speed and dispersion-relation calculations for continuous spectra (Lorentzian form) with fixed bandwidth, $\sigma = 0{\cdot}20$ and varying nonlinearity. (*a*) Dimensionless wavenumber spectra. (*b*) Normalized component phase speed as a function of wavenumber. (*c*) Normalized component phase speed as a function of frequency. (*d*) Normalized dispersion relation. □, $ka = 0{\cdot}01$; ○, $ka = 0{\cdot}10$; △, $ka = 0{\cdot}20$. ——, linear case.

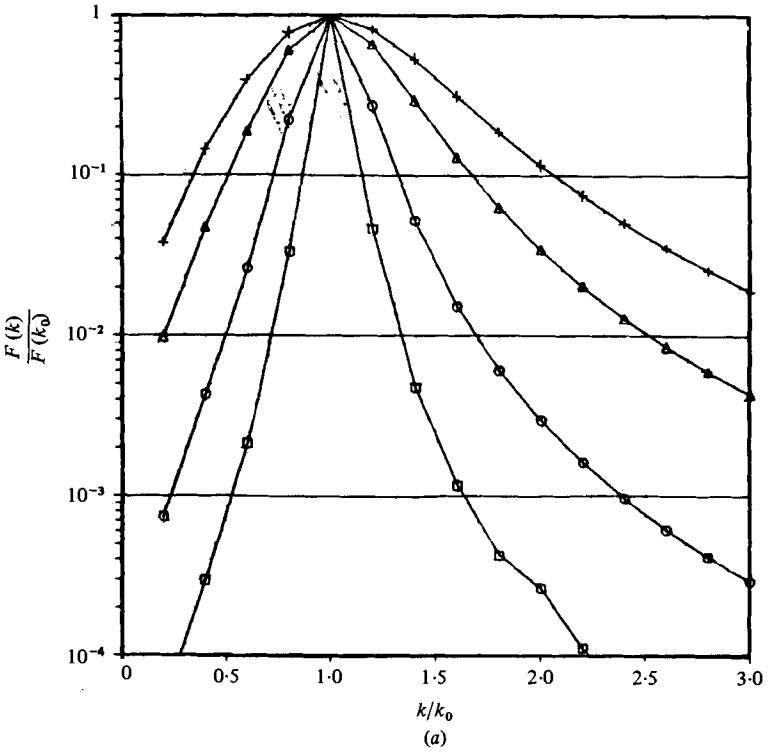

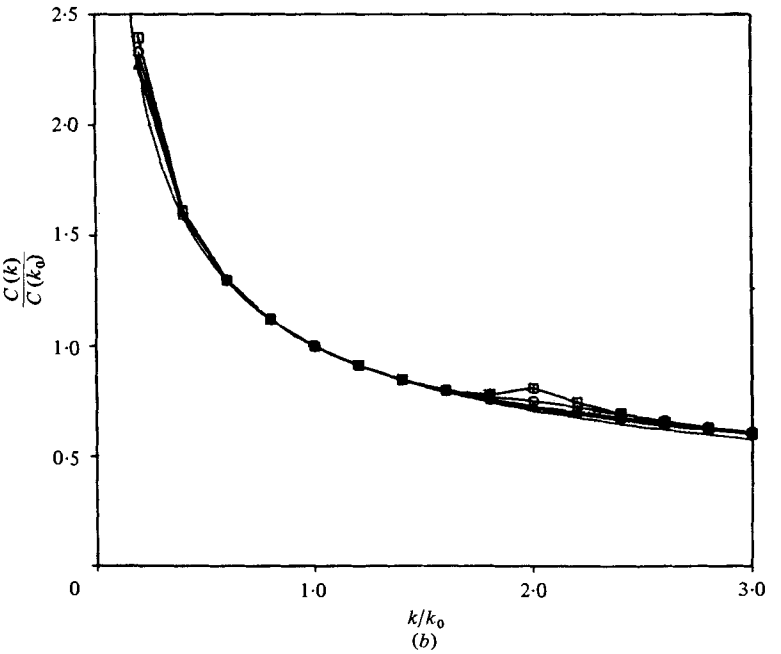

For legend for 5(*a*), (*b*) see p. 18.

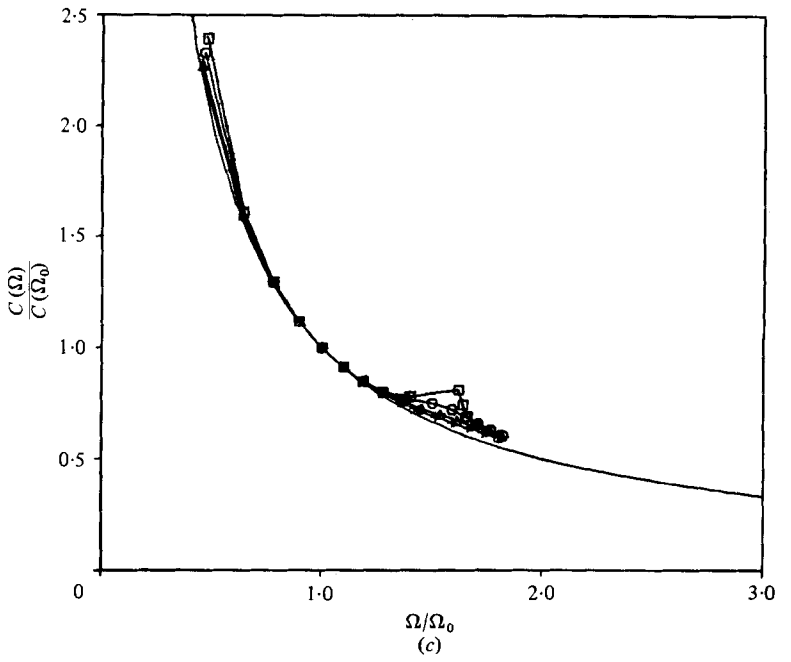

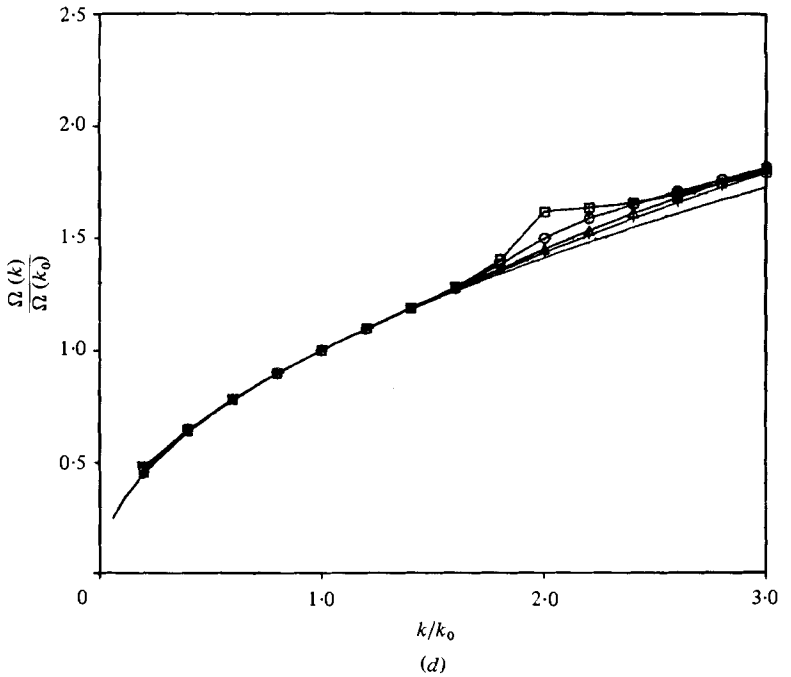

FIGURE 5. Component-phase-speed and dispersion-relation calculations for continuous spectra (Lorentzian form) with fixed nonlinearity $(ka)_{\text{rms}} = 0{\cdot}01$ and varying bandwidth. (*a*) Dimensionless wavenumber spectra. (*b*) Normalized component phase speed as a function of wavenumber. (*c*) Normalized component phase speed as a function of frequency. (*d*) Normalized dispersion relation. □, $\sigma = 0{\cdot}05$; ○, $\sigma = 0{\cdot}10$; △, $\sigma = 0{\cdot}20$; +, $\sigma = 0{\cdot}30$. ——, linear case.

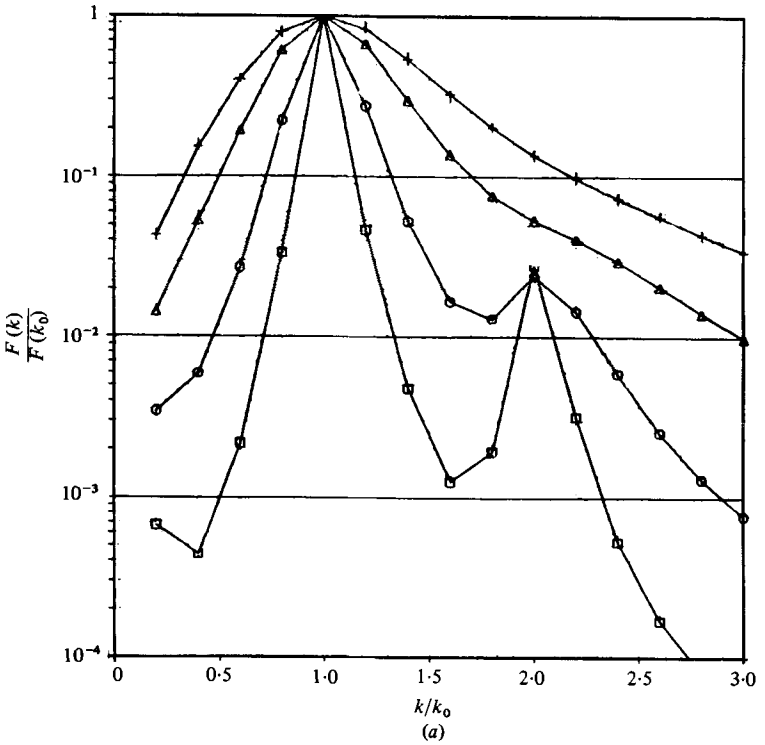

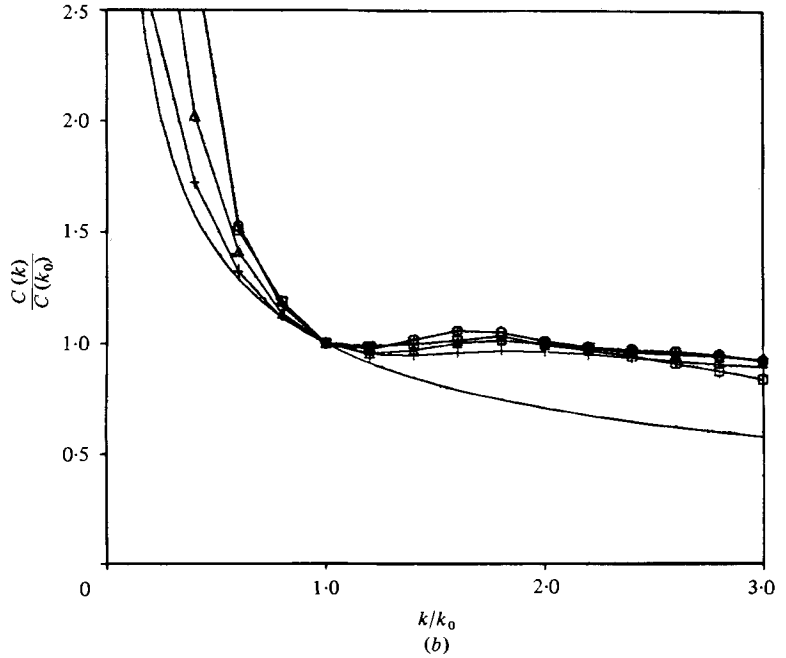

For legend for 6(*a*), (*b*) see p. 20.

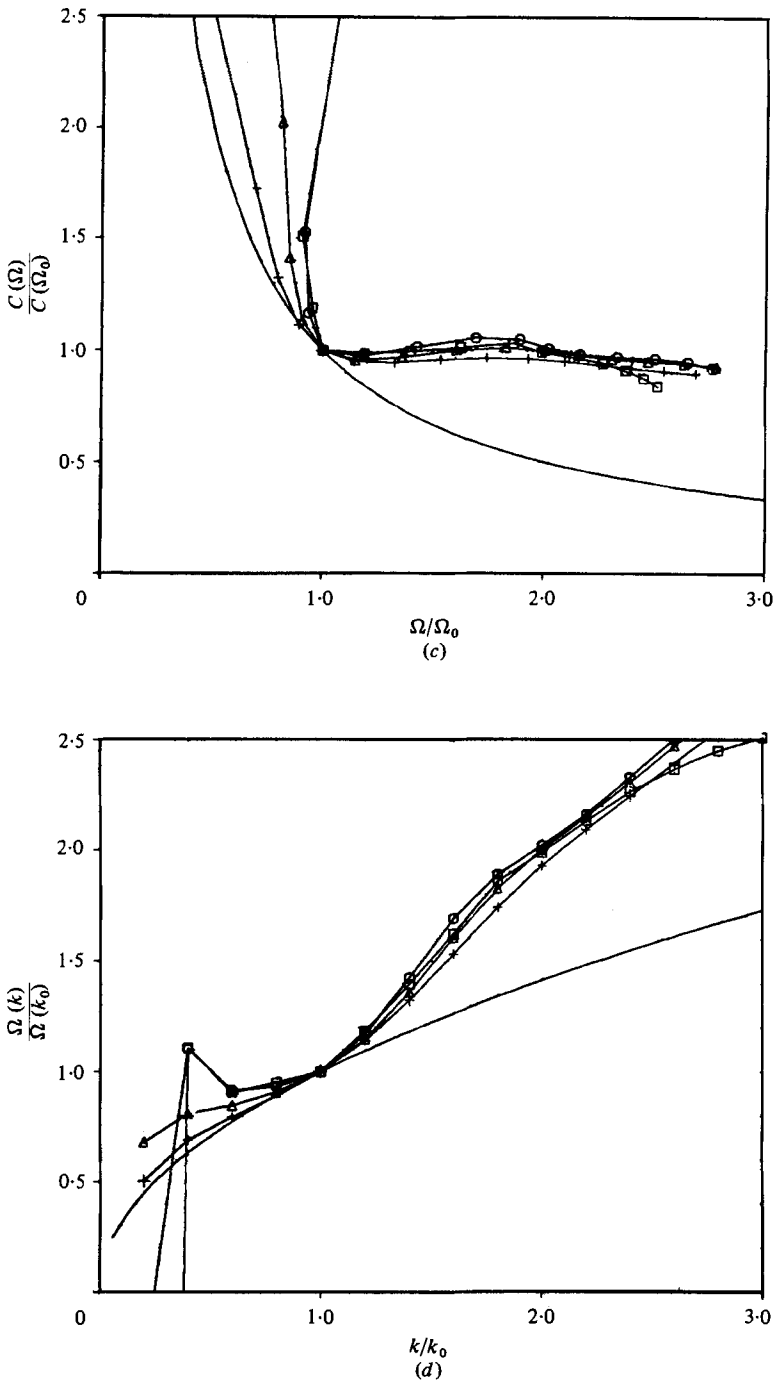

FIGURE 6. Component-phase-speed and dispersion-relation calculations for continuous spectra (Lorentzian form) with fixed nonlinearity $(ka)_{\text{rms}} = 0{\cdot}20$ and varying bandwidth. (*a*) Dimensionless wavenumber spectra. (*b*) Normalized component phase speed as a function of wavenumber. (*c*) Normalized component phase speed as a function of frequency. (*d*) Normalized dispersion relation. □, $\sigma = 0{\cdot}05$; ○, $\sigma = 0{\cdot}10$; △, $\sigma = 0{\cdot}20$; +, $\sigma = 0{\cdot}30$. ——, linear case.

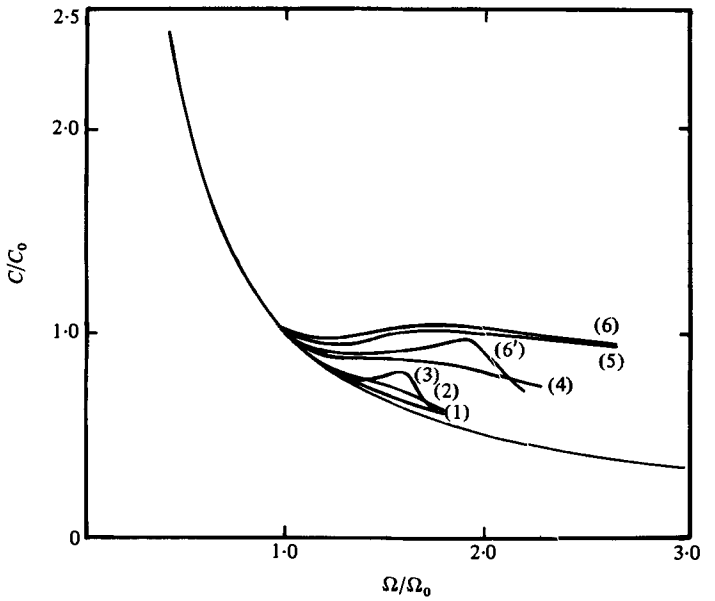

FIGURE 7. Normalized component phase speed C/C_0 versus dimensionless frequency Ω/Ω_0 for various spectra to illustrate the trend of results as a function of spectral aspect ratio $r = \sigma/(ka)_{\rm rms}$.

	$r = \sigma/(ka)_{\rm rms}$	$(ka)_{\rm rms}$	σ
(1)	30	0·01	0·30
(2)	10	0·01	0·10
(3)	5	0·01	0·05
(4)	2	0·10	0·20
(5)	1	0·20	0·20
(6)	0·5	0·20	0·10
(6′)	0·5	0·10	0·05

It has been proposed by Saffman & Yuen (1978) that the parameter

$$r = \frac{\sigma}{(ka)_{\rm rms}}, \tag{24}$$

which can be thought of as an effective 'aspect ratio' of the wave spectrum, may be used to characterize the properties of a wave system. When $r \gg 1$, the free wave components dominate the system, and the dispersion relation and related properties should be well described by the linear theory. When $r \ll 1$, the opposite should be true. In figure 7, we show the component phase speed for six different values of r. It can be seen that the departure from the linear theory generally increases with decreasing r, as expected. However, there is a difference between the broadband and the narrow-band cases. In the former case, the departure from linear theory is less localized than the latter even for the same or similar values of r [compare cases (2) with (3), and (6) with (6′)].

Summarizing, we find that the calculations support the proposition that departure from linear theory is most prominent when the spectrum is narrow-banded and the nonlinearity is relatively strong. The 'spectral aspect ratio' r defined in equation (24) provides a good qualitative measure of the departure from linear theory. Detailed features of the results are dependent on the particular values of σ and $(ka)_{\rm rms}$.

6. Comparison with experimental data

In the preceding sections, through analysis and numerical computation, some basic properties of the dispersion relation and component phase speed of wavetrains and wavefields have been established. Two types of wave components have been identified: the 'free' waves which more or less obey the linear dispersion relation, and the 'bound' components which couple nonlinearly with the dominant system, and do not obey the linear dispersion relation. For a modulated wavetrain, the higher modes are all bound components, and they show significant departure from the linear theory even for small values of wave steepness. For a general spectrum of waves, however, it is expected that both free and bound components are present. Examination of the dispersion relation and component phase speed for these 'mixed' systems shows that the bound-wave characteristics are more pronounced when the spectrum is narrow and the characteristic nonlinearity relatively strong, whereas the free components dominate when the opposite situation obtains.

Before comparison between calculated results and experimental data proceeds, it should be stressed again that the present purpose is limited to demonstrating the fact that nonlinear coupling can account for the type of phenomena observed in the laboratory and open ocean. The theory is highly idealized (one-dimensional, no wind, no current, fully deterministic), so the conclusions drawn from these comparisons between theory and data cannot definitely answer whether the balance of nonlinear and dispersion considered here is indeed the dominant mechanism in all of the experimental situations. On the other hand, good agreement should be suggestive that the mechanism considered is important in some circumstances.

There is another caveat. Strictly speaking, better comparisons of results could be made by using the definitions in equations (3)–(5) to relate $A(k)$ to the free surface. This would involve solving an integral equation. In this preliminary study, this initialization procedure has not been carried out; instead, the dominant part of the spectrum was fitted to obtain $A(k)$, and equation (5) was used to generate $B(k)$. The initial phase is arbitrarily set by letting $A(k)$ be real. This simplified procedure should be adequate to serve the present limited purpose.

The first set of comparisons shown is for a single, modulated wavetrain generated by a wave paddle (figure 8). In this plot, the calculated results for $k_0 a_0 = 0{\cdot}01$ and $k_0 a_0 = 0{\cdot}10$ are given and, considering the discussion in §4, little difference in the two cases is expected. Experimental data cover a range of $k_0 a_0$ from 0·02 to 0·10. As can be seen, the agreement between theory and experiment is very good; this supports the contention that, in a modulated wavetrain, all the higher modes are nonlinearly coupled to the primary. They do not obey the linear dispersion relation, regardless of how small the value of $k_0 a_0$ may be (experimentally, however, a practical difficulty arises for very small values of $k_0 a_0$, in that there is insufficient power in the higher harmonics to permit accurate determination of their phase speeds).

Next, some comparisons are shown between theory and experiments for a spectrum of waves in the absence of wind. Experimentally, these are produced by driving a programmable wave paddle with pre-recorded wind-wave amplitude wave forms. The frequency response of the wave paddle is flat to 5 Hz. Measurements are made at 30 feet downtank. The characteristic nonlinearity is varied from case to case by changing the amplitude gain of the wave paddle. Figure 9 shows a comparison for a

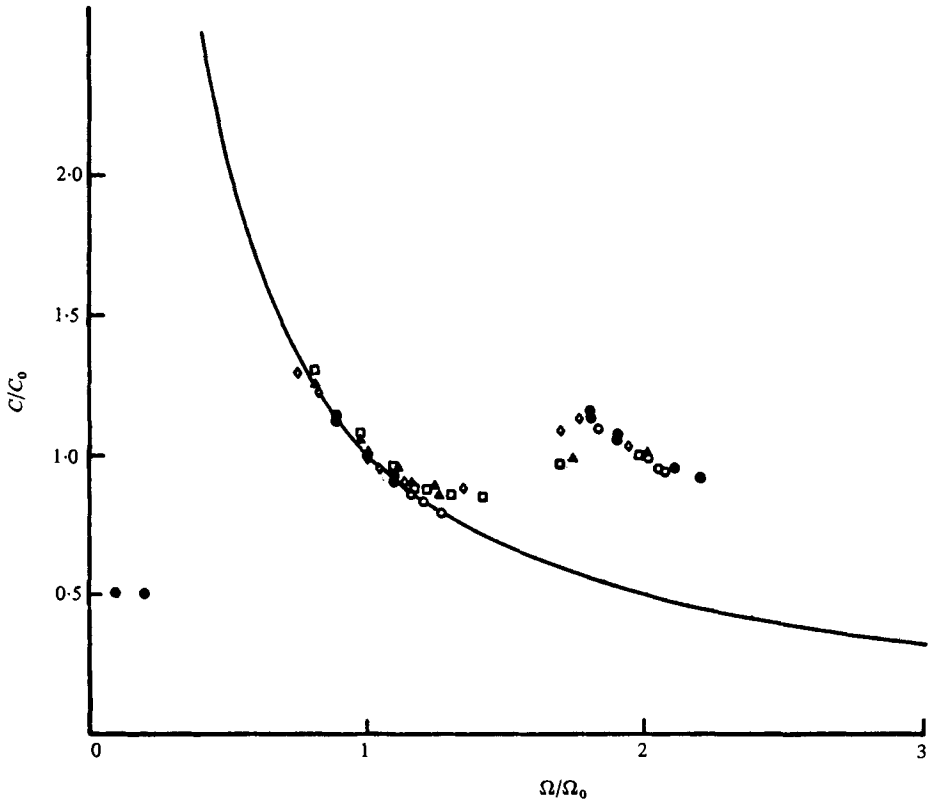

FIGURE 8. Comparison of calculations with experimental data for modulated wavetrains for a range of nonlinearity. Note that the results are insensitive to the values of k_0a_0. ●, nonlinear theory, $k_0a_0 = 0{\cdot}01, 0{\cdot}1$; ○, △, ◇, □, laboratory data (TRW), $0{\cdot}02 < k_0a_0 < 0{\cdot}1$. ——, linear theory.

spectrum with characteristic bandwidth σ/k_0 of 0·13, and characteristic nonlinearity k_0a_0 ranging from 0·01 to 0·098. It can be seen that the agreement is again very good. It must be noted, however, that some amount of ambiguity exists in the determination of the values of the spectral bandwidth, since the experimentally measured spectra are usually quite jagged and must be smoothed to yield a meaningful bandwidth. Nevertheless, the agreement remains satisfactory even when the upper and lower limits of the possible values are taken for the bandwidth.

For field experiments, attention is again focused on the range of wavenumbers between $k/k_0 = 0$ and $k/k_0 = 3$, where k_0 is the wavenumber at the peak of the spectrum, assuming a one-dimensional wavefield. Because of the dispersion relation, the range of Ω/Ω_0 is slightly smaller. Fifteen discrete points are used to fit the measured spectrum in this range. Results for the calculated phase speed and the dispersion relation are normalized by their values at k_0. This normalization scales out the drift velocity caused by a current, provided that the current equally affects all the waves considered. For a relatively narrow range of wavenumbers around the spectral peak, this normalization should remove the first-order effects of wind-induced drift quite effectively. A possible strong wavenumber dependence for shorter waves in the ripple and capillary regimes was not accounted for here, though, since it does not lie within our area of interest.

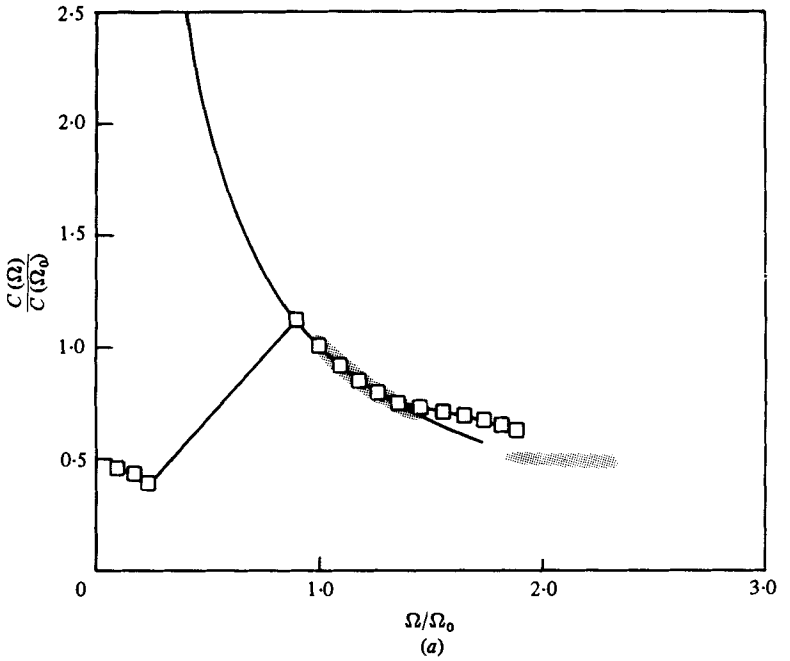

(*a*)

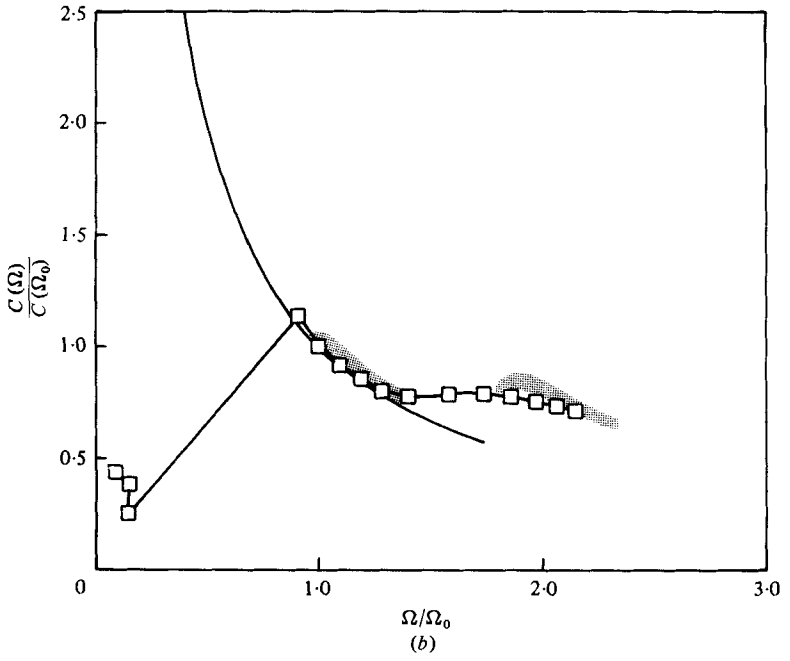

(*b*)

For legend for 9(*a*), (*b*) see p. 25.

Figure 10 shows the field data collected by Von Zweck (1970) in Buzzards Bay, Massachusetts, on the afternoon of 9 August 1968. The measured phase velocity is seen to be higher than that predicted by the linear theory. Von Zweck attributed this to directional effects rather than nonlinearity, since he noted that the typical wave slope was small, being around 10^{-2}. In figure 10, a calculation is shown with

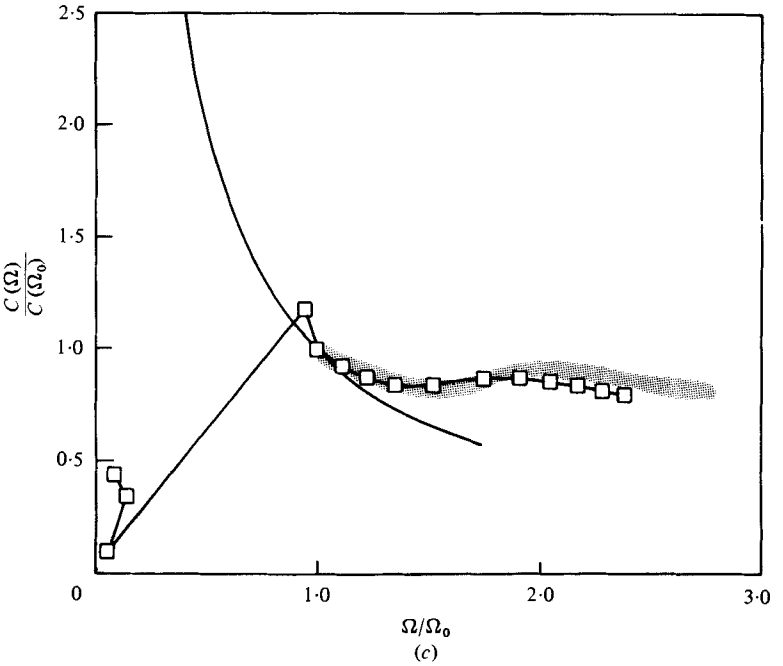

FIGURE 9. Comparison of calculations with experimental data for a spectrum of waves without wind. The data correspond to measurements in a wave tank at 30 ft from the wave paddle which is programmed to generate waves from prerecorded wind-wave data. The calculations are made with the Bretschneider spectra $\sigma = 0{\cdot}13$. (*a*) $k_0a_0 = 0{\cdot}01$. (*b*) $k_0a_0 = 0{\cdot}045$. (*c*) $k_0a_0 = 0{\cdot}098$. ——, linear case. The data are represented by the shaded areas.

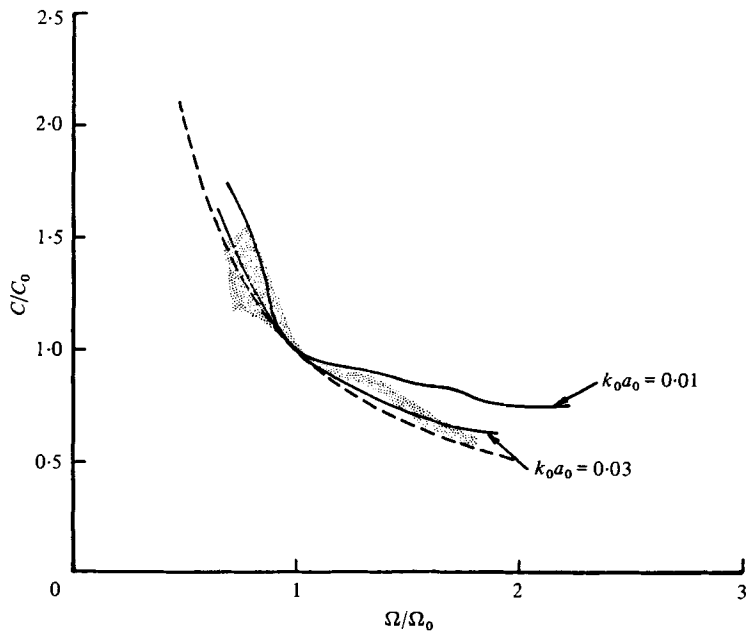

FIGURE 10. Comparison of calculations to ocean wind-wave data collected by Von Zweck (1970). The calculations are made with spectra obtained by fitting 15 points to the measured spectra. ▦, ocean data (Von Zweck 1970); ——, nonlinear theory, $k_0a_0 = 0{\cdot}03, 0{\cdot}10$; – – –, linear theory.

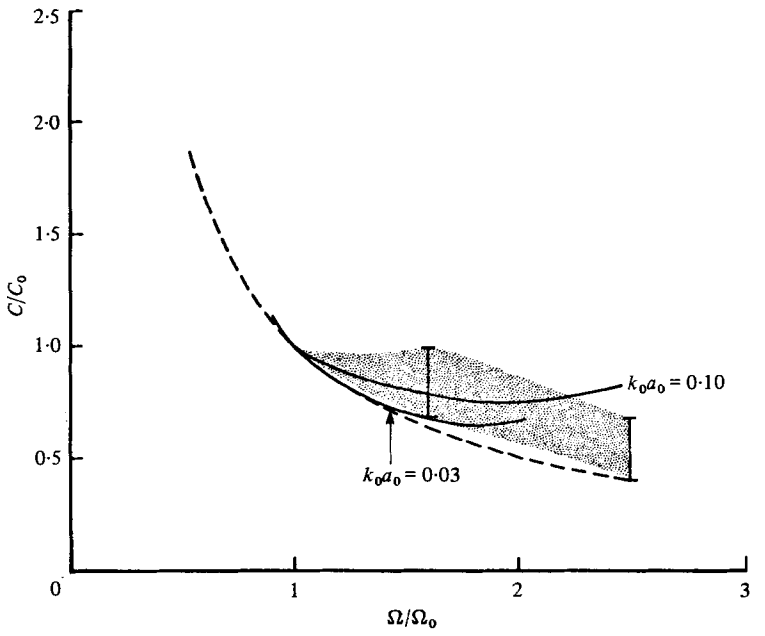

FIGURE 11. Comparison of calculations to ocean wind-wave data collected by Yefimov *et al.* (1972). The calculations are made with spectra obtained by fitting 15 points to the measured spectra. ▦, ocean data (Yefimov *et al.* 1972); ——, nonlinear theory, $k_0a_0 = 0{\cdot}03$, $0{\cdot}01$; – – –, linear theory.

$k_0a_0 = 3 \times 10^{-2}$, which matches the data. (A calculation with $k_0a_0 = 10^{-1}$ is also shown for comparison.) This is not meant to imply that directionality effects are not important (there are none at all in our calculations), but these results clearly show that nonlinearity is a possible candidate for explaining the departure from linear theory, even at this low value of k_0a_0.

The measurements made by Yefimov *et al.* (1972), in the Black Sea during the summer of 1970, are shown in figure 11. Only a portion of his data falls within our present range of interest. His data show substantial scatter, but they are consistently above the prediction of the linear theory. The typical wave-slope value quoted in his paper is about 0·03. The data would indeed be well matched by calculations with k_0a_0 between 0·03 and 0·1, with the assumption that the nonlinearity–dispersion balance is the only mechanism at work. Again, the agreement is interpreted to suggest that nonlinearity is a possible candidate for explaining the measured properties.

The ocean data collected by Grose *et al.* (1972) is considered next. It involves 204 observations in the Atlantic trade-wind region east of Barbados in 1968. For each observation, data were least-square fitted to a formula of the form

$$\Omega^a = bk,$$

where a and b are constants to be determined by the fit. For linear waves, a should be 2, and b the acceleration due to gravity in the appropriate units. Grose *et al.* found that the values for a range from 1·2 to 2·05, with the median at around 1·65. The consequences of their findings on the dispersion relation are shown in figure 12. The shaded

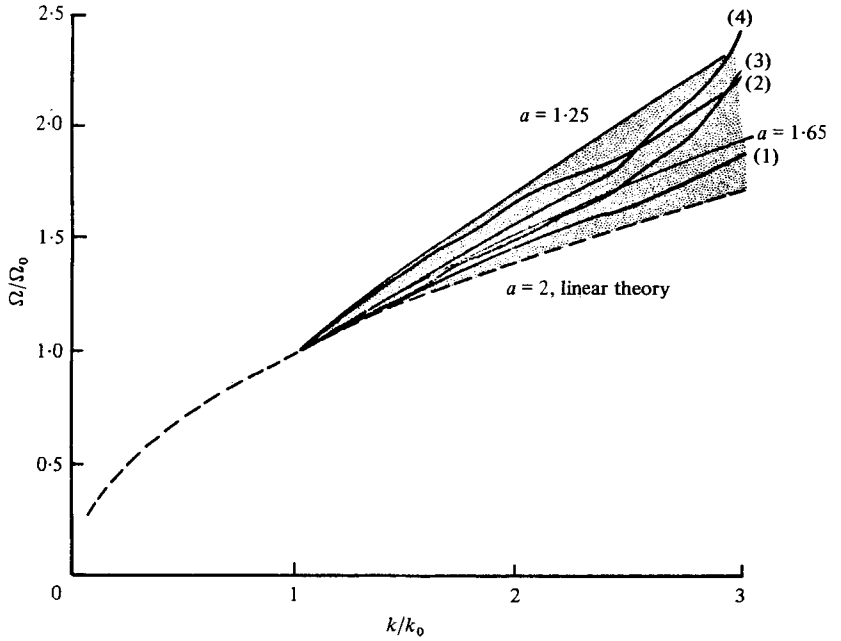

FIGURE 12. Comparison of calculations with ocean wind-wave data collected by Grose *et al.* (1972). The data are presented as dispersion-relation plots of the form $(\Omega/\Omega_0)^a = b(k/k_0)$, where a and b are determined by best fits. Calculations are made with spectra obtained by 15-point fitting of those given by Von Zweck and Yefimov lying within the range of parameters given by Grose *et al.* (1972). ▦, ocean data (Grose *et al.* 1972) with $\Omega^a = bk$. ——, nonlinear theory: (1), Von Zweck spectrum, $k_0a_0 = 0{\cdot}03$; (2), Von Zweck spectrum, $k_0a_0 = 0{\cdot}10$; (3), Yefimov spectrum, $k_0a_0 = 0{\cdot}07$; (4), Yefimov spectrum, $k_0a_0 = 0{\cdot}10$.

region represents the range of the dispersion curves for $a = 2$ (lower dashed curve) to $a = 1{\cdot}25$ (upper solid curve); and the curve corresponding to $a = 1{\cdot}65$ is given as a thin solid line. They quoted a typical value of k_0a_0 of about 0·065.

The spectral shapes for the dominant portion of the spectrum were not given in the paper, so their results will be compared only to the four calculations obtained using the Von Zweck spectrum with $k_0a_0 = 0{\cdot}03$ and 0·10, and the Yefimov spectrum with $k_0a_0 = 0{\cdot}7$ and 0·10. Figure 12 shows that the calculations lie within the data region, and suggests that the Yefimov spectrum with $k_0a_0 = 0{\cdot}07$ appears to yield the most typical results.

Finally, the laboratory and ocean data given by Ramamonjiarisoa & Giovanangeli (1978) are examined. The phase-speed data in figure 2 of their paper are replotted in figure 13, with the phase speed normalized at the dominant component. The laboratory data are represented by a shaded region and the two ocean measurements by hatched regions. The heavy line corresponds to a calculation using the Bretschneider spectrum (appendix C) with characteristic bandwidth 0·07 and characteristic nonlinearity $k_0a_0 = 0{\cdot}1$, a condition close to that found in the laboratory. The agreement is good, including a mild rise in the phase speed in the vicinity of the second harmonic, which is characteristic of a narrow spectrum. The two thin lines show the results obtained when the Yefimov spectrum (which is relatively broadband) with $k_0a_0 = 0{\cdot}03$ and 0·10 is used. They agree well with the measured ocean data, in spite of the fact that

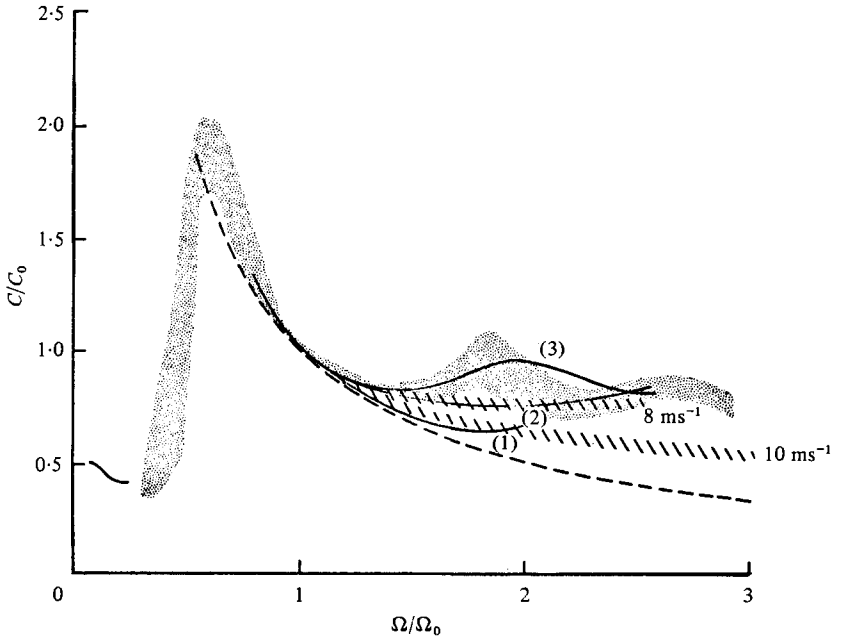

FIGURE 13. Comparisons of calculations with ocean and laboratory data collected by Ramamonjiarisoa & Giovanangeli (1978). ▦, laboratory data (Ramamonjiarisoa & Coantic 1976); ▨, ocean data (Ramamonjiarisoa & Giovanangeli 1978). ——, nonlinear theory: (1), Yefimov spectrum, $k_0a_0 = 0{\cdot}03$; (2), Yefimov spectrum, $k_0a_0 = 0{\cdot}07$; (3), Bretschneider, $\sigma = 0{\cdot}07$, $k_0a_0 = 0{\cdot}1$. – – –, linear theory.

the spectral shapes are not exactly matched. These comparisons demonstrate that the nonlinearity–dispersion balance, considered in this paper, may explain the difference in behaviour between laboratory and ocean data, as well as the departure of the measured results from linear theory.

7. Summary

The dispersion relation and component phase speeds of wave fields and modulated wavetrains have been calculated, assuming that the motion is one-space dimensional and deterministic in the absence of wind or drift currents. The objective is to assess the possibility that nonlinearity may account for the discrepancies that exist between various measurements and the linear theory.

Two types of wave behaviour have been identified: bound and free. The bound components are those generated through resonant wave interactions with the dominant system, and include the harmonics as special cases. They do not obey the linear dispersion relation; instead, they travel at speeds that are greater than the linear speeds and may be as great as the speeds of the dominant components in the system. Only the free components follow the dispersion relation closely. In a general wave system, both types of components are present, and the behaviour of the system depends on the relative importance of each type. This in turn has been found to depend on the nonlinearity and bandwidth of the wave system.

A parametric study has been performed, for a range of nonlinearity and bandwidths, to explore the detailed characteristics of wavefields and modulated wavetrains. The theory has been compared to laboratory and ocean measurements, and it has been found that the nonlinearity–dispersion balance is a likely candidate to account for both the discrepancy between the measurements and the linear theory as well as the difference in behaviour between laboratory and ocean measurements.

Because of assumptions made in our calculations, the results achieved are not to be taken as evidence that other effects, such as directionality, randomness and currents, are unimportant. However, there is sufficient evidence to support the contention that nonlinearity should not be ignored in any proposed theory for the evolution of ocean waves.

Appendix A. Third-order interaction coefficient

The third-order interaction coefficient $T_{i,j,k,m} = T(\mathbf{k}_i, \mathbf{k}_j, \mathbf{k}_l, \mathbf{k}_m)$ appearing in equation (1) was first found by Zakharov (1968), and is exhibited below with some minor misprints removed:

$$\begin{aligned} T_{0,1,2,3} = &-\frac{2V^{(-)}_{3,3-1,1}V^{(-)}_{0,2,0-2}}{\omega_{1-3}-\omega_3+\omega_1} - \frac{2V^{(-)}_{2,0,2-0}V^{(-)}_{1,1-3,3}}{\omega_{1-3}-\omega_1+\omega_3} \\ &-\frac{2V^{(-)}_{2,2-1,1}V^{(-)}_{0,3,0-3}}{\omega_{1-2}-\omega_2+\omega_1} - \frac{2V^{(-)}_{3,0,3-0}V^{(-)}_{1,1-2,2}}{\omega_{1-2}-\omega_1+\omega_2} \\ &-\frac{2V^{(-)}_{0+1,0,1}V^{(-)}_{2+3,2,3}}{\omega_{2+3}-\omega_2-\omega_3} - \frac{2V^{(+)}_{-2-3,2,3}V^{(+)}_{0,1,-0-1}}{\omega_{2+3}+\omega_2+\omega_3} + W_{0,1,2,3}, \end{aligned} \tag{A 1}$$

where $k_i = |\mathbf{k}_i|$, $\omega_i = \omega(k_i)$, and $V_{i,j,l} = V(\mathbf{k}_i, \mathbf{k}_j, \mathbf{k}_l)$ is given by

$$\begin{aligned} V^{(\pm)}_{0,1,2} = \frac{1}{8\pi\sqrt{2}}\Bigg\{&[\mathbf{k}_0\cdot\mathbf{k}_1 \pm k_0k_1]\left[\frac{\omega_0\omega_1}{\omega_2}\frac{k_2}{k_0k_1}\right]^{\frac{1}{2}} \\ &+[\mathbf{k}_0\cdot\mathbf{k}_2 \pm k_0k_2]\left[\frac{\omega_0\omega_2}{\omega_1}\frac{k_1}{k_0k_2}\right]^{\frac{1}{2}} \\ &+[\mathbf{k}_1\cdot\mathbf{k}_2 + k_1k_2]\left[\frac{\omega_1\omega_2}{\omega_0}\frac{k_0}{k_1k_2}\right]^{\frac{1}{2}}\Bigg\} \end{aligned} \tag{A 2}$$

(note that $V^{(\pm)}_{0,1,2} \neq V^{(\mp)}_{-0,1,2}$), and $W_{i,j,l,m} = W(\mathbf{k}_i, \mathbf{k}_j, \mathbf{k}_l, \mathbf{k}_m)$ is given by

$$\begin{aligned} W_{0,1,2,3} = &\overline{W}_{-0,-1,2,3} + \overline{W}_{2,3,-0,-1} - \overline{W}_{2,-1,-0,3} \\ &- \overline{W}_{-0,2,-1,3} - \overline{W}_{-0,3,2,-1} - \overline{W}_{3,-1,2,-0}, \end{aligned} \tag{A 3}$$

with

$$\overline{W}_{0,1,2,3} = \frac{1}{64\pi^2}\left[\frac{\omega_0\omega_1}{\omega_2\omega_3}k_0k_1k_2k_3\right]^{\frac{1}{2}}\{2(k_0+k_1) - k_{1+3} - k_{1+2} - k_{0+3} - k_{0+2}\}, \tag{A 4}$$

and

$$k_{i\pm j} = |\mathbf{k}_i \pm \mathbf{k}_j|; \quad \omega_{i\pm j} = \omega(k_{i\pm j}).$$

Appendix B. Calculation of B and $\partial B/\partial t$

If it is assumed that the spectrum $A(\mathbf{k}, 0)$ is one-dimensional and real, and that $A(k, 0) = 0$ for $k < 0$, then equation (5) can be written as

$$B(k_p, t) = -\int_0^\infty \left\{ V^{(-)}_{p,1,p-1} A_1 A_{p-1} \frac{\exp[i(\omega_p - \omega_1 - \omega_{p-1})t]}{\omega_p - \omega_1 - \omega_{p-1}} + 2V^{(-)}_{1,p,1-p} A_{1-p} A_1 \frac{\exp[i(\omega_p - \omega_1 + \omega_{1-p})t]}{\omega_p - \omega_1 + \omega_{1-p}} + V^{(+)}_{p,1,-p-1} A_1 A_{-p-1} \frac{\exp[i(\omega_p + \omega_1 + \omega_{-p-1})t]}{\omega_p + \omega_1 + \omega_{-p-1}} \right\} dk_1.$$

Therefore, for $k_p > 0$,

$$B(k_p, 0) = -\int_0^{k_p} \frac{V^{(-)}_{p,1,p-1} A_1 A_{p-1}}{\omega_p - \omega_1 - \omega_{p-1}} dk_1 - \int_{k_p}^\infty \frac{2V^{(-)}_{1,p,1-p} A_{1-p} A_1}{\omega_p - \omega_1 + \omega_{1-p}} dk_1,$$

$$B(-k_p, 0) = -\int_0^\infty \frac{2V^{(-)}_{1,-p,1+p} A_{1+p} A_1}{\omega_p - \omega_1 + \omega_{1+p}} dk_1 - \int_0^{k_p} \frac{V^{(+)}_{-p,1,p-1} A_1 A_{p-1}}{\omega_p + \omega_1 + \omega_{p-1}} dk_1.$$

Similarly,

$$\frac{\partial B}{\partial t}(k_p, 0) = -i\int_0^{k_p} V^{(-)}_{p,1,p-1} A_1 A_{p-1} dk_1 - i\int_{k_p}^\infty 2V^{(-)}_{1,p,1-p} A_{1-p} A_1 dk_1,$$

$$\frac{\partial B}{\partial t}(-k_p, 0) = -i\int_0^\infty 2V^{(-)}_{1,-p,1+p} A_{1+p} A_1 dk_1 - i\int_0^{k_p} V^{(+)}_{-p,1\ p-1} A_1 A_{p-1} dk_1.$$

Since $A(k, 0)$ is real, $B(\pm k_p, 0)$ is real and $\partial B(\pm k_p, 0)/\partial t$ is imaginary. For assumed spectral forms for $A(k, 0)$ the terms $B(\pm k_p, 0)$, $\partial A(k_p, 0)/\partial t$, and $\partial B(\pm k_p, 0)/\partial t$ can be calculated by integration.

Appendix C. Spectral forms used in the calculations

The spectra were chosen so that the peak occurs at the wavenumber k_0. The integrated non-dimensional spectrum is normalized so that

$$\int_0^\infty \hat{F}\left(\frac{k}{k_0}\right) d\left(\frac{k}{k_0}\right) = 1. \tag{C 1}$$

The spectral width $\tilde{\sigma}$ is defined by the location where the spectrum drops to one-half of its peak value:

$$\hat{F}\left(1 \pm \frac{\tilde{\sigma}}{k_0}\right) = \tfrac{1}{2}\hat{F}(1). \tag{C 2}$$

The actual value of $\tilde{\sigma}$ is obtained by Taylor expansion of (C 2) to second order. The dimensionless bandwidth σ is $\tilde{\sigma}/k_0$.

The phase speed was calculated using a Lorentzian and a generalized Pierson–

Moskowitz spectrum (Bretschneider spectrum). The non-dimensional Lorentzian spectrum is given by

$$\hat{F}\left(\frac{k}{k_0}\right) = 2\alpha\left(\frac{k}{k_0}\right) \Big/ \left[\left(\frac{k}{k_0} - \frac{2k_0^2 - 2\tilde{\sigma}^2}{3k_0^2 - \tilde{\sigma}^2}\right)^2 + \frac{4\tilde{\sigma}^2(4k_0^2 - 3\tilde{\sigma}^2)}{(2k_0^2 - \tilde{\sigma}^2)^2}\right]^2, \tag{C 3}$$

where

$$\alpha = \frac{4\tilde{\sigma}^2(4k_0^2 - 3\tilde{\sigma}^2)}{(2k_0^2 - \tilde{\sigma}^2)^2} \Big/ \left\{1 + \frac{2k_0^2 - 3\tilde{\sigma}^2}{2\tilde{\sigma}(4k_0^2 - 3\tilde{\sigma}^2)^{\frac{1}{2}}}\left[\frac{\pi}{2} + \tan^{-1}\frac{2k_0^2 - 3\tilde{\sigma}^2}{2\tilde{\sigma}(4k_0^2 - 3\tilde{\sigma}^2)^{\frac{1}{2}}}\right]\right\}, \tag{C 4}$$

is a coefficient that is used to normalize the spectrum.

In terms of dimensional quantities the spectrum is given by

$$F(k) = \frac{\langle \eta^2 \rangle}{k_0} \hat{F}\left(\frac{k}{k_0}\right), \tag{C 5}$$

where $\langle \eta^2 \rangle$ is the mean-squared amplitude, which is equal to the integral of the spectral function $F(k)$:

$$\langle \eta^2 \rangle = \int_0^\infty F(k)\, dk. \tag{C 6}$$

The Bretschneider spectrum is given by

$$\hat{F}\left(\frac{k}{k_0}\right) = \frac{\beta}{(k/k_0)^\beta} \exp\left[-\frac{\beta}{\beta - 1}\left(\frac{k}{k_0}\right)^{1-\beta}\right], \tag{C 7}$$

where β is related to the width of the spectrum $\tilde{\sigma}$ and the wavenumber k_0 at the spectral peak by

$$\beta = \tfrac{1}{2} + \tfrac{1}{2}(1 + 4k_0^2/\tilde{\sigma}^2)^{\frac{1}{2}}. \tag{C 8}$$

REFERENCES

Benjamin, T. B. & Feir, J. E. 1967 The disintegration of wave trains in deep water. Part 1. Theory. *J. Fluid Mech.* **27**, 417–430.

Crawford, D. R., Lake, B. M., Saffman, P. G. & Yuen, H. C. 1981 Stability of weakly nonlinear deep-water waves in two and three dimensions. *J. Fluid Mech.* **105**, 177–191.

Crawford, D. R., Saffman, P. G. & Yuen, H. C. 1980 Evolution of a random inhomogeneous field of nonlinear deep-water gravity waves. *Wave Motion* **2**, 1–16.

Grose, P. L., Warsh, K. L. & Garstang, M. 1972 Dispersion relations and wave shapes. *J. Geophys. Res.* **77**, 3902–3906.

Hasselmann, K. 1962 On the nonlinear energy transfer in a gravity-wave spectrum. Part 1. General theory. *J. Fluid Mech.* **12**, 481–500.

Hasselmann, K. 1963 On the nonlinear energy transfer in a gravity-wave spectrum, 2. Conservation theorems, wave–particle correspondence, irreversibility. *J. Fluid Mech.* **15**, 273–281.

Huang, N. E. & Tung, C. C. 1977 The influence of the directional energy distribution on the nonlinear dispersion relation in a random gravity wave field. *J. Phys. Oceanog.* **7**, 403–414.

Lake, B. M. & Yuen, H. C. 1978 A new model for nonlinear wind waves. Part 1. Physical model and experimental evidence. *J. Fluid Mech.* **88**, 33–62.

Masuda, A., Kuo, Y. Y. & Mitsuyasu, H. 1979 On the dispersion relation of random gravity waves. Part 1. Theoretical framework. *J. Fluid Mech.* **92**, 717–730.

Mitsuyasu, H., Kuo, Y. Y. & Masuda, A. 1979 On the dispersion relation of random gravity waves. Part 2. An experiment. *J. Fluid Mech.* **92**, 731–749.

Mollo-Christensen, E. & Ramamonjiarisoa, A. 1978 Modeling the presence of wave groups in a random wave field. *J. Geophys. Res.* C **83**, 4117–4122.

PLANT, W. J. & WRIGHT, J. W. 1979 Spectral decomposition of short gravity wave systems. *J. Phys. Oceanog.* **9**, 621–624.

RAMAMONJIARISOA, A. 1974 Thèse de Doctorat d'Etat, Université de Provence, enregistrée au C.N.R.S. no. A.0.10.023.

RAMAMONJIARISOA, A. & COANTIC, M. 1976 Loi expérimentale de dispersion des vagues produites parle vent sur une faible longueur d'action. *C. R. Acad. Sci. Paris* B **282**, 111–113.

RAMAMONJIARISOA, A. & GIOVANANGELI, J. P. 1978 Observations de la vitesse de propagation des vagues engendrées par le vent au large. *C. R. Acad. Sci. Paris* B **287**, 133–136.

RIKIISHI, K. 1978 A new method for measuring the directional wave spectrum. Part II. Measurement of the directional spectrum and phase velocity of laboratory wind waves. *J. Phys. Oceanog.* **8**, 518–529.

SAFFMAN, P. G. & YUEN, H. C. 1978 Nonlinear deep-water waves. VII. Multiple time scales approach to nonlinear interactions in a gravity wave field. *TRW Rep.* no. 31326-6038-RU-00.

VON ZWECK, O. H. 1970 Observations of propagation characteristics of a wind driven sea. Doctorate thesis, Massachusetts Institute of Technology.

YEFIMOV, V. V., SOLOV'YEV, Y. P. & KHRISTOFOROV, G. N. 1972 Observational determination of the phase velocities of spectral components of wind waves. *Atmospheric & Ocean Phys.* **8**, 435–446.

YUEN, H. C. & LAKE, B. M. 1978 A new model for nonlinear wind waves. Part 2. Theoretical model. *Stud. Appl. Math.* **60**, 261–270.

ZAKHAROV, V. E. 1968 Stability of periodic waves of finite amplitude on the surface of a deep fluid. *J. Appl. Mech. Tech. Phys.* **9**, 86–94.